Award Number: 99HQGR0098

GROUND MOTION ATTENUATION RELATIONS FOR THE CENTRAL AND EASTERN UNITED STATES

FINAL REPORT, JUNE 30, 2001

P. Somerville, N. Collins, N. Abrahamson*, R. Graves, and C. Saikia

URS Group, Inc.

566 El Dorado Street
Pasadena, CA 91101

Tel: (626) 449-7650
Fax: (626) 449-3536

*PG&E
245 Market Street
San Francisco, CA 94105

Email: paul_somerville@urscorp.com

Research supported by the U.S. Geological Survey (USGS), Department of the Interior, under award number 99HQGR0098. The views and conclusions contained in this document are those of the authors and should not be interpreted as necessarily representing the official policies, either expressed or implied, of the U.S. Government.

Award Number: 99HQGR0098

GROUND MOTION ATTENUATION RELATIONS FOR THE CENTRAL AND EASTERN UNITED STATES

FINAL REPORT, JUNE 30, 2001

P. Somerville, N. Collins, N. Abrahamson*, R. Graves, and C. Saikia

URS Group, Inc.
566 El Dorado Street
Pasadena, CA 91101
Tel: (626) 449-7650, Fax: (626) 449-3536

*PG&E, 245 Market Street, San Francisco, CA 94105

Email: paul_somerville@urscorp.com

ABSTRACT

We have developed ground motion attenuation relationships for the central and eastern United States for use in future revisions of the National Seismic Hazard maps produced by the USGS. The ground motion attenuation relations describe the dependence of the strength of the ground motions on the earthquake magnitude and on the distance from the earthquake. We first developed earthquake source scaling relations for use in generating ground motions. The source models have spatially varying slip distributions on the fault plane, and are described by self-similar scaling relations between seismic moment and source parameters such as fault dimensions and rise time derived from the slip models of three recent earthquakes in eastern Canada. We generated suites of ground motion time histories using these source scaling relations. The broadband time histories are calculated using a representative crustal structure model and ranges of source parameter values consistent with the source scaling relations. These broadband simulations were used to generate ground motion attenuation relations for hard rock conditions in the central and eastern United States. Ground motion models for both the horizontal and vertical component were developed for response spectral acceleration in the period range of 0 to 4 seconds. Separate ground motion models were developed for earthquake depth distributions that correspond to rifted and non-rifted domains.

EARTHQUAKE SOURCE MODELS FOR EASTERN NORTH AMERICA

Detailed studies of the spatial distribution of slip on the fault plane for 15 crustal earthquakes in tectonically active regions, derived from strong motion recordings and other data, have shown that the slip distribution is highly variable, characterized by asperities (regions of large slip) surrounded by regions of low slip. These slip models were used to develop relationships between seismic moment and a set of fault parameters that are needed for predicting strong ground motions (Somerville et al., 1999). These parameters include fault length, fault width, rise time (duration of slip at a point on the fault), and the size, slip contrast and location of asperities. Hartzell et al. (1994) obtained detailed models of the distribution of slip on the fault for three earthquakes in eastern North America: the 1983 Miramichi, 1988 Saguenay and 1989 Ungava earthquakes. The slip models of these three earthquakes are characterized by strong spatial variation in slip over the fault surface, like those of earthquakes in tectonically active regions.

We analyzed the rupture models of the Miramichi, Saguenay and Ungava earthquakes using procedures similar to those used by Somerville et al. (1999) to analyze the rupture models of earthquakes in tectonically active regions. The source parameters of the earthquakes are listed in Tables 1 through 3. The rupture areas were derived from the rupture models of Hartzell et al. (1994) by the trimming procedure described by Somerville et al. (1999), and the rise times were derived from the predominant duration of rupture on fault elements. These rise time values are lower than those in Table 6 of Hartzell et al. (1994) for the reasons given in the footnotes below Table 1.

Table 1. Source Parameters of Crustal Earthquakes

Earthquake, Location	Date	Mech.	Mo x 10^{24} dyne-cm	Mw	Slip Duration (sec)	Rupture Area (km^2)
Miramichi, New Brunswick	1982.1.9	RV	2.0	5.5	0.6*	17
Saguenay, Quebec	1988.11.25	RV	6.1	5.8	0.5**	33
Ungava, Quebec	1989.12.25	RV	13.0	6.0	0.9***	33

* combined duration of the two slip episodes of 0.2 and 0.4 sec
** duration of slip of the central asperity
*** duration of slip representative of 29 of 33 fault elements that do not have large shallow slip

Table 2. Dimensions and Discretization of Fault Planes *

Earthquake	T	B	L	R	length (km)	width (km)	nx	ny	dx (km)	dy (km)	kx_{max} (km^{-1})	ky_{max} (km^{-1})
Miramichi	2	3	1	2	5.0	3.375	5	3	1.0	1.125	0.5	0.444
Saguenay	2	1	3	2	5.0	6.667	5	6	1.0	1.11	0.5	0.45
Ungava	0	3	0	2	13.0	3.0	13	3	1.0	1.0	0.5	0.5

* T, B, L, and R in the first 4 columns refer to the numbers of rows trimmed from the top (T) and bottom (B) of the slip model, and from the left side (L) and right side (R) of the slip model.

Table 3. Orientation of Fault Planes

Earthquake	depth of top (km)	depth of bottom (km)	dip	strike	slip model reference
Miramichi	5.72	8.31	50^o	170^o	Hartzell et al., 1984
Saguenay	24.0	30.0	65^o	320^o	Hartzell et al., 1984
Ungava	0.5	2.5	42^o	50^o	Hartzell et al., 1984

The three events are not sufficient to constrain the slopes of the scaling relations, so we assume that they are self-similar, consistent with Somerville et al. (1987) and Somerville et al. (1999). The relation between seismic moment and rupture area is shown at the top of Figure 1, and the relation between seismic moment and rise time is shown at the bottom of Figure 1. The relation between seismic moment derived from these three recent earthquakes is consistent with data from two sets of mostly larger, older eastern North American events. The first is a set of 13 earthquakes in the magnitude range of 4.5 to 6.9

that occurred between 1925 and 1983. For these earthquakes, Somerville et al. (1987) obtained a relationship between seismic moment and source duration, which provides an indirect relationship between seismic moment and fault rupture area, shown as the long dashed line in the top of Figure 1. The second is a set of four large historical earthquakes, the three 1811-1812 New Madrid events and the 1886 Charleston event, whose seismic moments and rupture areas were estimated by Johnston (1996).

In Figure 1, we also show the relations for crustal earthquakes in tectonically active regions derived by Somerville et al. (1999). The rupture areas of the eastern North American earthquakes are 0.4 times as large and the rise times are 1.85 times longer than those of the earthquakes in tectonically active regions. The average fault displacement of the eastern events is 2.5 times larger, and for constant slip velocity we would expect the rise time to similarly be 2.5 times longer, not 1.85 times longer, than for events in tectonically active regions. Our data are too few to rule out a rise time that is 2.5 times longer, but we have chosen to retain the scaling relation that best fits the data, corresponding to a rise time that is 1.85 times longer.

The parameters of individual asperities, analyzed using the methods described in Somerville et al. (1999), are listed in Table 4 which also shows a comparison of their average properties with those of earthquakes in tectonically active regions. The eastern North American events tend to have fewer but larger asperities than earthquakes in tectonically active regions. However, all three events have quite small fault dimensions, which may make it difficult to resolve small asperities. We consider that the overall characteristics of the asperities are sufficiently similar to those of earthquakes in tectonically active regions that the asperity scaling relations of the latter earthquakes, adjusted for differences if fault area, can be used to represent the asperity characteristics of eastern North American events.

Table 4. Asperity Parameters of eastern North American earthquakes

Earthquake	No. Of Asperities	Area of Largest Asperity km^2		Combined Area of Asperities km^2		Average Slip Contrast of Asperities
Miramichi	2	2.25	0.13	3.38	0.20	2.12
Saguenay	1	6.67	0.20	6.67	0.20	2.32
Ungava	1	16.0	0.41	16.0	0.41	1.85
Average*	1.3 (2.6)		0.25 (0.16)		0.27 (0.22)	2.10 (2.01)

* value in parentheses is for earthquakes in tectonically active regions (Somerville et al., 1999).

The source scaling relations for eastern North American earthquakes derived from these analyses are listed in Table 5. These relations, which we used in modeling strong ground motions in Task 2, allow us to construct earthquake source models without resorting to a priori assumptions about the shape of the source spectrum, as is done in the stochastic approach. There is currently debate among proponents of the stochastic method as to whether the source spectrum is best represented by a Brune spectrum with a single corner frequency (Toro et al., 1997), or by a model having two corner frequencies (Boatwright and Choy, 1992; Atkinson, 1993). In Figure 2, we show a sample of five slip models for a magnitude 7 reverse faulting earthquake derived using the parameters listed in Table 5.

Table 5. Scaling Relations of Slip Models of Crustal Earthquakes in Eastern North America

Rupture Area vs. Seismic Moment:	$A = 8.9 \times 10^{-16} \times M_o^{2/3}$
Average Slip vs. Seismic Moment:	$D = 3.9 \times 10^{-7} \times M_o^{1/3}$
Combined Area of Asperities vs. Seismic Moment*	$A_a = 2.0 \times 10^{-16} \times M_o^{2/3}$
Area of Largest Asperity vs. Seismic Moment*	$A_l\ (km^2) = 1.4 \times 10^{-16} \times M_o^{2/3}$
Radius of Largest Asperity vs. Seismic Moment*	$r_l\ (km) = 6.7 \times 10^{-9} \times M_o^{1/3}$
Average Number of Asperities*	2.6
Area of Fault Covered by Asperities*	0.22
Average Asperity Slip Contrast*	2.0
Hypocentral Distance to Center of Closest Asperity Vs.Moment*	$R_A = 1.35 \times 10^{-8} \times Mo^{1/3}$
Slip Duration vs. Seismic Moment	$T_R = 3.75 \times 10^{-9} \times Mo^{1/3}$
Spatial Wavenumber Along Strike (1/km)*	log kx = 1.92 - 0.5 M
Spatial Wavenumber Down Dip (1/km)*	log ky = 2.13 - 0.5 M

* assumed to be the same as for shallow crustal earthquakes in tectonic regions

In stable continental interiors, there is a clear difference in the rate, maximum magnitude, and maximum depth of seismicity in rifted and non-rifted domains (EPRI, 1994; Johnston, 1996). Rifted domains include continental margins, such as the Charleston source zone, and failed rifts, such as the Reelfoot Rift. Rifted domains have more frequent, larger, and deeper earthquakes. In non-rifted domains, the seismicity is concentrated in a narrow depth range of 0 - 10 km, and occurs within an overall depth extent of 0 - 30 km. By contrast, in rifted domains, the seismicity is concentrated over a broad depth range of 5 - 30 km, and occurs within an overall depth range of 0 - 35 km.

The continental margin rifted domain in eastern North America lies at the edge of the continent along the Atlantic coast. The system of failed rifts that lies west of the continental margin includes the St. Lawrence (part of the Iapetan margin) and branches such as the Saguenay Graben and the Ottawa rift; the Reelfoot Rift; and the Southern Oklahoma Aulacogen (Wheeler, 1995; Wheeler and Johnston, 1992; Wheeler and Frankel, 2000). The locations of the rifted domains in eastern North America are represented approximately by the eastern and western margins of the Phanerozoic Rim Zone described by Wheeler and Frankel (2000) and shown in their Figure 1.

Many of the largest earthquakes in central and eastern North America occurred in or near rifted domains. These include the New Madrid, Charleston, and numerous Charlevoix events. They also include two earthquakes that occurred at depths of about 25 km: the magnitude Mw 5.4 southern Illinois earthquake of November 9, 1968 (Somerville et al., 1987), and the magnitude Mw 5.7 Saguenay, Quebec earthquake of November 25, 1988 (Somerville et al., 1990). These two earthquakes suggest the potential for faulting extending to large depths in large earthquakes occurring in rifted domains in central and eastern North America. The 2001 Bhuj, India earthquake may be an example of an earthquake that ruptured the full depth range of seismicity in a rifted domain. Accordingly, we have developed ground motion attenuation relations for two depth distributions: one for non-rifted domains, where seismicity is concentrated at shallow depths, and the other for rifted domains, where seismicity occurs over a wider and deeper depth range.

Strong Motion Simulations

We developed ground motion attenuation relations for use in eastern North America using simulated ground motion time histories. In Table 6, we list the source parameters used to simulate ground motion time histories.

Table 6. Parameters for Ground Motion Simulations

PARAMETER	RANGE OF VALUES
Magnitude	Mw 6.0 - 7.5
Other Source Parameters	Scaling with magnitude is described in Table 4
Distance	0 - 500 km
Crustal Structure	Midcontinent model: α, β, ρ, Q (h) (see Table 7); K = 0.006
Site Condition	Hard Rock (Vs = 2.83 km/sec)
Centroid Depth	Approx. 5.0, 10, and 20.0 km
Mechanism	Reverse
Site Locations	Equally spaced radially about the top center of the fault

To simulate ground motion time histories, we use a broadband Green's function method that has a rigorous basis in theoretical and computational seismology and has been extensively validated against recorded strong motion data (Somerville et al., 1996). The earthquake source is represented as a shear dislocation on an extended fault plane, whose radiation pattern, and its tendency to become subdued at periods shorter than about 0.5 sec, are accurately represented. Wave propagation is represented rigorously by Green's functions computed for the seismic velocity structure that contains the fault and the site, or by empirical Green's functions derived from strong motion recordings of small earthquakes. These Green's functions contain both body waves and surface waves. The ground motion time history is calculated in the time domain using the elastodynamic representation theorem. This involves integration over the fault surface of the convolution of the slip time function on the fault with the Green's function for the appropriate depth and distance. To simulate broadband time histories, the ground motions are computed separately in the short period and long period ranges, and then combined into a single broadband time history. The use of different methods in these two period ranges is necessitated by the observation that ground motions have fundamentally different characteristics in these two period ranges.

Ground motions are simulated by the summation of contributions from subevents on a grid of fault elements on a rectangular fault. In our simulations, the source functions for these fault elements are derived from strong motion recordings of a magnitude 5.5 earthquake. According to the scaling models of Irikura (1983) and Joyner and Boore (1986), this summation process is robust when simulating magnitudes about one magnitude unit or more larger than the magnitude of the subevent. We consider our simulations for magnitude 6.5 and larger to be robust. The simulations for magnitude 6 may have amplitudes that are biased low, but the shapes of their spectra and their attenuation with distance are considered to be reliable, so they were used to constrain the shape but not the level of the ground motion model.

The crustal structure model used in the simulations, given in Table 7, is the Mid-continent structure that we developed in the course of the EPRI (1993) project. In that project, we regionalized the crustal structure of the central and eastern United States into 16 regions. The ground motion attenuation characteristics of one of these 16 regions, the Mid-continent region, was found to be most closely representative of the attenuation characteristics of these 16 regions.

In Figure 3, we show a profile of simulated strong motion accelerograms for a magnitude 7 reverse faulting earthquake. The profile crosses the north-striking fault from east to west. The peak accelerations are higher on the hanging wall (east side) than on the foot wall (west side of the fault). The accelerograms in Figure 3 are normalized to their peak values.

Table 7. Mid-Continent Crustal Structure Model

Depth to Top (km)	Thickness (km)	P wave vel. (km/sec)	S wave vel. (km/sec)	Density (gm/cc)	P wave Q	S wave Q
0	1	4.9	2.83	2.52	1000.0	500.0
1	11	6.1	3.52	2.71	1500.0	750.0
12	28	6.5	3.75	2.78	2000.0	1000.0
40	-	8.0	4.62	3/35	2500.0	1250.0

In Figure 4, we show the attenuation of peak acceleration with distance for a large suite of simulations of a magnitude 7 earthquake including those shown in Figure 3. The simulations are for three different fault depths, three different hypocenter locations, ten different slip models, and 127 different station locations, for a total of 11,430 simulations. The peak accelerations are compared with the attenuation models of Toro et al. (1997). This model uses approximate methods to represent the effects of crustal structure on ground motion attenuation, and so it does not show the decrease in the rate of attenuation beyond 100km, seen in the simulations, which is caused by critical reflections from the lower crust. Our broadband simulation approach provides a more realistic representation of the effect of crustal structure on ground motion attenuation than does the Toro et al. (1997) model. Shallow depth of faulting tends to cause larger ground motions at close distances, but at larger distances the ground motions tend to be smaller due to larger critical distances for lower crustal reflections.

GROUND MOTION ATTENUATION RELATIONSHIPS FOR THE CENTRAL AND EASTERN UNITED STATES

Ground Motion Model Parameterization

Ground motion characteristics depend not only on the seismic moment and distance of the earthquake, as is commonly represented in empirical ground motion attenuation relations, but also on such parameters as the orientation, style of faulting, and depth of the fault, and the location of the hypocenter and the recording station. Examples of these effects include rupture directivity effects (Somerville et al., 1997) and hanging wall effects (Abrahamson and Somerville, 1996). However, in most regions of eastern North America, it is not possible to identify active faults as potential seismic sources. Instead, the earthquakes are assumed to occur in a distributed way over broad regions. The detailed representation of ground motion effects that are specific to the location and orientation of faults is therefore of secondary importance for ground motion prediction.

Accordingly, we developed a simplified ground motion model whose purpose is predicting ground motions where fault locations and orientations are not known. In this model, seismic moment Mw is the sole source parameter and Joyner-Boore distance is the only station location parameter. The Joyner-Boore distance is the closest horizontal distance to the vertical surface projection of the fault plane (Abrahamson and Shedlock, 1997). The ground motion model is for hard rock site conditions.

We developed models for two depth distributions: rifted and non-rifted domains. As described above, in non-rifted domains, the seismicity is concentrated in a narrow depth range of 0 - 10 km, and occurs within an overall depth extent of 0 - 30 km, while in rifted domains, the seismicity is concentrated over a broad depth range of 5 - 30 km, and occurs within an overall depth range of 0 - 35 km.

To more rigorously represent the different ground motion characteristics of the rifted and non-rifted domains, we could also take account of the differences in crustal structure in these two domains, described by EPRI (1993), in which eastern North America was divided into 16 regions of differing crustal structure. Among these regions, the failed rift domains tend to have larger crustal thickness and a stronger velocity increase at the Conrad layer, giving rise to differences in ground motion attenuation. However, for this study, we have used a single crustal structure model that best represents the average attenuation characteristics in eastern North America, for simplicity of application in seismic hazard calculations. The difference in the depth distribution of seismicity is the only feature of the differences between rifted and non-rifted domains that we have used in generating the distinct ground motion models for rifted and non-rifted domains.

The ground motion simulations for a range of focal depths were weighted using depth distributions that are representative of these two domains. For the non-rifted domains, the simulations for centroid depths of 5, 10 and 20 km were given equal weight. For the rifted domains, the simulations for centroid depth of 10 km were given a weight of 1/3, and the simulations for a depth of 20 km were given a weight of 2/3. Depth is not a predictive parameter in the ground motion model, so we use closest horizontal distance to the surface projection of the fault as the distance measure for this model.

We used the random effects model of Abrahamson and Youngs (1992) to develop the ground motion model. The functional form of the model, given in Table 8, follows Abrahamson and Silva (1997), with a modification to allow for a change in slope. We found this decrease in slope to occur at a distance of 50 km. The value of the constant h in the term ln (h + c) was found to be 6 km, the same as in Abrahamson and Silva (1997).

Table 8. Form of the Ground Motion Attenuation Relations

For $r < r_1$

$$\ln Sa(g) = c_1 + c_2(M - m_1) + c_3 \ln R + c_4(M - m_1) \ln R + c_5 r + c_7(8.5 - M)^2$$

For $r \geq r_1$

$$\ln Sa(g) = c_1 + c_2(M - m_1) + c_3 \ln R_1 + c_4(M - m_1) \ln R + c_5 r + c_6(\ln R - \ln R_1) + c_7(8.5 - M)^2$$

where

Sa(g)	is spectral acceleration in g
m_1	= 6.4
r_1	= 50 km
h	= 6 km
R	$= \sqrt{r^2 + h^2}$
R_1	$= \sqrt{r_1^2 + h^2}$
M	is moment magnitude
R	= Joyner Boore distance

Table 9. Coefficients of the Ground Motion Attenuation Relations

Nonrift Zone - Horizontal							
Period	**c1**	**c2**	**c3**	**c4**	**c5**	**c6**	**c7**
0.01	0.418	0.808	-0.728	0.0651	-0.00601	-0.301	0.0000
0.04	1.099	0.808	-0.728	0.0651	-0.00601	-0.301	0.0000
0.10	1.071	0.808	-0.728	0.0651	-0.00601	-0.301	0.0000
0.20	0.978	0.808	-0.728	0.0651	-0.00601	-0.301	0.0000
0.40	0.851	0.808	-0.728	0.0651	-0.00538	-0.423	-0.0518
1.00	-0.139	0.808	-0.739	0.0651	-0.00398	-0.659	-0.1020
2.00	-0.932	0.808	-0.754	0.0651	-0.00318	-0.702	-0.1400
4.00	-2.080	0.808	-0.686	0.0651	-0.00156	-0.762	-0.1956
Rift Zone - Horizontal							
0.01	0.239	0.805	-0.679	0.0861	-0.00498	-0.477	0.0000
0.04	0.926	0.805	-0.679	0.0861	-0.00498	-0.477	0.0000
0.10	0.888	0.805	-0.679	0.0861	-0.00498	-0.477	0.0000
0.20	0.793	0.805	-0.679	0.0861	-0.00498	-0.477	0.0000
0.40	0.622	0.805	-0.664	0.0861	-0.00468	-0.557	-0.0518
1.00	-0.307	0.805	-0.696	0.0861	-0.00362	-0.755	-0.1020
2.00	-1.132	0.805	-0.728	0.0861	-0.00221	-0.946	-0.1400
4.00	-2.282	0.805	-0.671	0.0861	-0.000381	-1.059	-0.1956
Nonrift Zone - Vertical							
0.01	-0.151	0.8535	-0.607	0.0905	-0.00536	-0.490	0.0000
0.04	0.518	0.8535	-0.607	0.0905	-0.00536	-0.490	0.0000
0.10	0.505	0.8535	-0.607	0.0905	-0.00536	-0.490	0.0000
0.20	0.536	0.8535	-0.607	0.0905	-0.00536	-0.490	0.0000
0.40	0.566	0.8535	-0.682	0.0905	-0.00480	-0.698	0.0000
1.00	-0.273	0.8535	-0.781	0.0905	-0.00405	-0.658	-0.0115
2.00	-1.314	0.8535	-0.767	0.0905	-0.00348	-0.570	-0.0240
4.00	-2.382	0.8535	-0.712	0.0905	-0.00207	-0.490	-0.0565
Rift Zone - Vertical							
0.01	-0.530	0.936	-0.500	0.0746	-0.00436	-0.642	0.0000
0.04	0.147	0.936	-0.500	0.0746	-0.00436	-0.642	0.0000
0.10	0.122	0.936	-0.500	0.0746	-0.00436	-0.642	0.0000
0.20	-0.050	0.936	-0.500	0.0746	-0.00436	-0.642	0.0000
0.40	-0.222	0.936	-0.512	0.0746	-0.00397	-0.732	0.0000
1.00	-1.030	0.936	-0.569	0.0746	-0.00357	-0.708	-0.0115
2.00	-1.693	0.936	-0.705	0.0746	-0.00295	-0.629	-0.0240
4.00	-2.430	0.936	-0.744	0.0746	-0.00152	-0.614	-0.0565

Table 10. Uncertainty in the Ground Motion Model (natural log units)

Nonrift Zone - Horizontal				
Period	**Parametric-a**	**Parametric-b**	**Modeling**	**Total**
0.01	0.2652	0.39	0.35	0.587
0.04	0.2761	0.39	0.35	0.592
0.10	0.2828	0.39	0.35	0.595
0.20	0.3151	0.39	0.35	0.611
0.40	0.2963	0.39	0.35	0.602
1.00	0.4535	0.39	0.35	0.693
2.00	0.6365	0.39	0.35	0.824
4.00	0.7432	0.39	0.35	0.909
Rift Zone - Horizontal				
0.01	0.2652	0.39	0.35	0.587
0.04	0.2761	0.39	0.35	0.592
0.10	0.2828	0.39	0.35	0.595
0.20	0.3151	0.39	0.35	0.611
0.40	0.2963	0.39	0.35	0.602
1.00	0.4535	0.39	0.35	0.693
2.00	0.6365	0.39	0.35	0.824
4.00	0.7432	0.39	0.35	0.909
Nonrift Zone - Vertical				
0.01	0.3284	0.39	0.35	0.618
0.04	0.3270	0.39	0.35	0.618
0.10	0.3345	0.39	0.35	0.622
0.20	0.3579	0.39	0.35	0.635
0.40	0.4337	0.39	0.35	0.680
1.00	0.5551	0.39	0.35	0.763
2.00	0.6791	0.39	0.35	0.858
4.00	0.7553	0.39	0.35	0.919
Rift Zone - Vertical				
0.01	0.3284	0.39	0.35	0.618
0.04	0.3270	0.39	0.35	0.618
0.10	0.3345	0.39	0.35	0.622
0.20	0.3579	0.39	0.35	0.635
0.40	0.4337	0.39	0.35	0.680
1.00	0.5551	0.39	0.35	0.763
2.00	0.6791	0.39	0.35	0.858
4.00	0.7553	0.39	0.35	0.919

Method of Development of the Ground Motion Models.

Primary magnitude scaling (c2 term)

We used simulations for the magnitude range 6.0 to 7.5 to develop the model. As described above, the simulations for magnitude 6 are biased low, but the shapes of their spectra and their attenuation with distance are considered to be reliable. Accordingly, we did not allow the magnitude 6 simulations to constrain the magnitude scaling term c2, but they constrained the other terms.

Magnitude scaling of spectral shape (c7 term)

Some models (e.g. Abrahamson and Silva, 1997) use different primary magnitude scaling in different magnitude ranges, with larger scaling at smaller magnitudes. The narrow magnitude range of our simulations does not allow us to evaluate this. Instead, we followed the assumption made by most other models that the primary magnitude scaling applies at all magnitudes, and forced all scaling of spectral shape with magnitude to be represented by the c7 term. The simulations were not sufficient to constrain this term, so we used the values of the Abrahamson and Silva (1997) model, which are similar to those of the Atkinson and Boore (1995) model.

Smoothing of Model Coefficients

We smoothed the period dependence of the coefficients in the following sequence. First, we smoothed the c7 coefficients (the Abrahamson and Silva (1997) values) by setting the values for periods shorter than 0.2 second to zero. Next, the magnitude scaling coefficients c2 and c4, which do not interact, were assumed to be period independent, and each were set to a value averaged over all periods. Next, the c3 term, which controls the slope at distances less than 50 km, was smoothed to an average value for periods between 0.01 and 0.4 seconds for the horizontal component and 0.01 and 0.2 seconds for the vertical component. Next, the c6 term, which controls the slope at distances beyond 50 km, was smoothed to an average value for periods between 0.01 and 0.2 seconds. The c5 term, which represents the effects of Q, was smoothed in the same manner as the c6 term. The c1 term, which scales the overall level of the ground motions, did not require smoothing. The smoothed coefficients are listed in Table 9, and shown in Figures 5 and 6.

Representation of Uncertainty in Ground Motions

To be optimally useful in seismic hazard calculations, the attenuation relations need to include comprehensive representation of uncertainty. The parameters that need to be specified include the median value (μ) of the ground motion parameter, the scatter (σ) about the median value, and the uncertainty in each of these two values (σ_μ and σ_σ). The median values are obtained from the equation listed in Table 8 using the coefficients in Table 9. The values of σ_μ and σ_σ are estimated to be 0.2 and 0.15 natural log units respectively, based on our work for the Trial Implementation Project (Savy, 1997).

The variability (σ) of the ground motion model, expressed as the natural logarithm of the standard error, is given in Table 10. The variability was estimated using the procedure described by Abrahamson et al. (1992). Two categories of variability are accounted for. Modeling uncertainty, measured by the difference between recorded and simulated ground motions, represents the discrepancy between the actual physical processes and the simplified representation of them in the model. Parametric uncertainty represents the uncertainty in the values of the model parameters in future earthquakes. The total uncertainty is obtained from the combination of these two components.

The estimate of modeling uncertainty used in this project is representative of that obtained from the simulation of recorded strong ground motions of earthquakes in the magnitude range of 6.5 to 7.5 whose source parameters are well known (e.g. Somerville et al. 1996). The modeling uncertainty, which is listed in Table 10, is approximately independent of period.

The estimate of parametric uncertainty was obtained from two sources. One source consists of the parameters that were varied in the simulations performed for this project. These include the distribution of slip on the fault, the location of the hypocenter, the location of the recording station with respect to the fault (including differences between ground motions on the foot wall and hanging wall of the fault), and the source depth. The combined contribution of variations in these source parameters is listed under the heading of Parametric-a in Table 10. This component of the parametric uncertainty increases with period, reflecting the transition from more stochastic source and wave propagation effects in the short period component of the simulations, to more deterministic effects in the long period simulations.

In developing the rift model, we used simulations for two depth ranges instead of the three used for the non-rifted model, and doubled the weight given to the simulations for the deepest earthquakes. This resulted in an artificially lower variability for the rifted model. Accordingly, we used the parametric uncertainty of the non-rifted model to represent the parametric uncertainty of the rifted model.

The other estimate of parametric uncertainty relates to source parameters that were varied by us in previous studies but not in this study. These parameters include variations in crustal structure, which contribute a standard error of 0.2 natural log units (EPRI, 1993); variations in rupture area for a given seismic moment (static stress drop), which contribute a standard error of 0.28 natural log units (EPRI, 1993); and rise time and rupture velocity, which contribute a standard error of 0.15 and 0.10 natural log units respectively (Ostuka et al., 1998). The combined parametric uncertainty due to variations in these parameters, 0.39 natural log units, is listed in Table 10 under the heading Parametric-b.

The total uncertainty in the ground motion model, listed in the right hand column of Table 10, is obtained by the square root of the sum of the squares (SRSS) combination of all of the above contributions to uncertainty.

Description of Ground Motion Models

We used the procedures described above to develop ground motion models for both horizontal and vertical ground motions in non-rifted and rifted domains. The coefficients of these models are listed in Table 9, and the standard errors are listed in Table 10.

The model for horizontal ground motions in non-rifted domains is displayed in Figures 7 through 13. Figures 7 through 11 show the attenuation of spectral acceleration with distance for various periods for each of several magnitudes. In these figures, the individual simulation values, which are for a range of different source depths, are shown in addition to the model, and the model is compared with the Atkinson and Boore (1995) and Toro et al. (1997) models. Figures 12 and 13 show horizontal response spectra for a range of magnitudes for each of several distances, comparing the model with the Atkinson and Boore (1995) and Toro et al. (1997) models respectively. Figure 14 shows the model for the vertical component.

The attenuation of peak ground motion for Mw 6.5 in non-rifted and rifted domains is compared in Figures 15 and 16 for the horizontal and vertical components respectively. The differences between

the horizontal components are small (less than 10%), but the vertical ground motions for rifted domains are significantly lower than those of non-rifted domains, as low as two-thirds the non-rifted values at very close distances. This is mainly attributed to the deeper depth distribution of the rifted domain. The fact that a comparable difference does not occur in the horizontal component indicates that the depth effect is offset by other effects, which may be related to geometrical spreading.

The attenuation of horizontal and vertical ground motions for Mw 6.5 is compared in Figures 17 and 18 for non-rifted and rifted domains respectively. Generally, the horizontal component is larger than the vertical component, especially at distances less than 50 km, but beyond 50 km the differences are small. The relatively large vertical component is due to the fact that the high surface velocity causes the S wave to have a shallow incidence angle, causing a large component of the S wave to appear on the vertical component.

The response spectra of the models are displayed in Figures 19 through 22. The horizontal and vertical response spectra of the non-rift and rift models are compared in Figures 19 and 20, and the non-rift and rift models for the horizontal and vertical respectively are shown in Figures 21 and 22.

Acknowledgments

The ground motion model was developed with the assistance of Norm Abrahamson, Nancy Collins, and Robert Graves. The authors would like to thank Norm Abrahamson and PG&E for their contribution to this project.

References

Abrahamson, N.A. and W.J. Silva (1997). Empirical response spectral attenuation relations for shallow crustal earthquakes. *Seismological Research Letters* 68, 94-127.

Abrahamson, N.A. and K.M. Shedlock (1997). Overview of attenuation relations special issue. *Seismological Research Letters* 68, 9-23.

Abrahamson, N.A. and P.G. Somerville (1996). Effects of the hanging wall and footwall on ground motions recorded during the Northridge Earthquake, *Bull. Seism. Soc. Am.*, 86, S93-S99.

Abrahamson, N.A. and R.R. Youngs (1992). A stable algorithm for regression analysis using the random effects model. *Bull. Seism. Soc. Am.* 82, 505-510.

Abrahamson, N.A., P.G. Somerville, and C. Allin Cornell (1990). Uncertainty in numerical strong motion predictions, *Proc. 4th U.S. National Conference on Earthquake Engineering*, **1**, 407-416.

Atkinson. G.M and D.M. Boore (1996). New ground motion relations for eastern North America. *Bull. Seism. Soc. Am.* 85, 17-30.

Atkinson, G. (1993). Source spectra for earthquakes in eastern North America. *Bull. Seism. Soc. Am.* 83, 1778-1798.

Boatwright, J. and G. Choy (1992). Aceleration source spectra anticipated for large earthquakes in eastern North America, *Bull. Seism. Soc. Am.*, 82, 660-682.

Electric Power Research Institute (1994). The earthquakes of stable continental regions. Report EPRI TR-102261-V1.

Electric Power Research Institute (1993). Guidelines for determining design basis ground motions. Volume 1. Method and guidelines for estimating earthquake ground motion in eastern North America. Report EPRI TR-102293.

Frankel, A., C. Mueller, T. Barnhard, D. Perkins, E. Leyendecker, N. Dickman, S. Hanson and M. Hopper (1996). National Seismic Hazard Maps, June 1996. *U.S. Geological Survey Open File Report* 96-532.

Hartzell, S., C. Langer and C. Mendoza (1994). Rupture histories of eastern North American earthquakes. *Bull. Seism. Soc. Am.* 84, 1703-1724.

Irikura, K. (1983). Semi-empirical estimation of strong ground motions during large earthquakes, *Bull. Disaster Prevention Res. Inst. (Kyoto Univ).* 33, 63-104.

Johnston, A.C. (1996). Seismic moment assessment of earthquakes in stable continental regions:
I. Instrumental seismicity, Geophys. J. Int. 124, 381-414.
II. Historical seismicity, Geophys. J. Int. 125, 639-678.
III. New Madrid 1811-1812, Charleston 1886 and Lisbon 1755, Geophys. J. Int. 126, 314-344.

Joyner, W.B. and D.M. Boore (1986). On simulating large earthquakes by Green's function addition of smaller earthquakes, in: Proceedings of the 5th Maurice Ewing Symposium on Earthquake Source Mechanics, American Geophysical Union, p. 269-274.

Ohtsuka, H., P.G. Somerville, and T. Sato (1998). Estimation of broadband strong ground motions considering uncertainty of fault parameters, J. Struct. Mech. Earthq. Eng., JSCE, No.584/I-42, 185-200.

Saikia, C.K., P.G. Somerville, H.K. Thio, N.F. Smith, A. Pitarka, B.B. Woods (1998). Crustal structure and ground motion models in the eastern and Central United States from National Seismograph Network Data. NUREG/CR-6593, U.S. Nuclear Regulatory Commission.

Savy, J. (1997). Ground motion attenuation in eastern North America. Section 4.3 of Report on Trial SHAC Methodology Implementation Project, Lawrence Livermore National Laboratory.

SSHAC (1996). Probabilistic seismic hazard analysis: a consensus. Senior Seismic Hazard Analysis Committee, USDOE, USNRC, EPRI.

Somerville, P.G., K. Irikura, R. Graves, S. Sawada, D. Wald, N. Abrahamson, Y. Iwasaki, T. Kagawa, N. Smith and A. Kowada (1999). Characterizing earthquake slip models for the prediction of strong ground motion. *Seismological Research Letters* 70, 59-80.

Somerville, P.G., N.F. Smith, R.W. Graves, and N.A. Abrahamson (1997). Modification of empirical strong ground motion attenuation relations to include the amplitude and duration effects of rupture directivity, *Seismological Research Letters* 68, 199-222.

Somerville, P.G., C.K. Saikia, D.J. Wald, and R.W. Graves (1996). Implications of the Northridge earthquake for strong ground motions from thrust faults, *Bull. Seism. Soc. Am.* 86, S115-S125.

Somerville, P.G., J.P. McLaren, L.V. LeFevre, R.W. Burger and D.V. Helmberger (1987). Comparison of source scaling relations of eastern and western North American earthquakes, *Bull. Seism. Soc. Am.*, **77**, 332-346.

Toro, G.R., N.A. Abrahamson, and J.F. Schneider (1997). Model of strong ground motions from earthquakes in eastern North America: best estimates and uncertainties, *Seismological Research Letters* 68, 41-57.

Wheeler, R.L. (1995). Earthquakes and the cratonward limit of Iapetan faulting in eastern North America, *Geology* 23, 105-108.

Wheeler, R.L. and A. Frankel (2000). Geology in the 1996 USGS seismic hazard maps, central and eastern United States. *Seismological Research Letters* 71, 273-282.

Wheeler, R.L. and A.C. Johnston (1992). Geologic implications of earthquake source parameters in central and eastern North America, *Seismological Research Letters* 63, 491-514.

BIBLIOGRAPHY

Somerville, P.G. (2001). Ground motion attenuation relations for the central and eastern United States. Proceedings of the second ATC-35 National Earthquake Ground Motion Mapping Workshop, San Francisco, May 10-11.

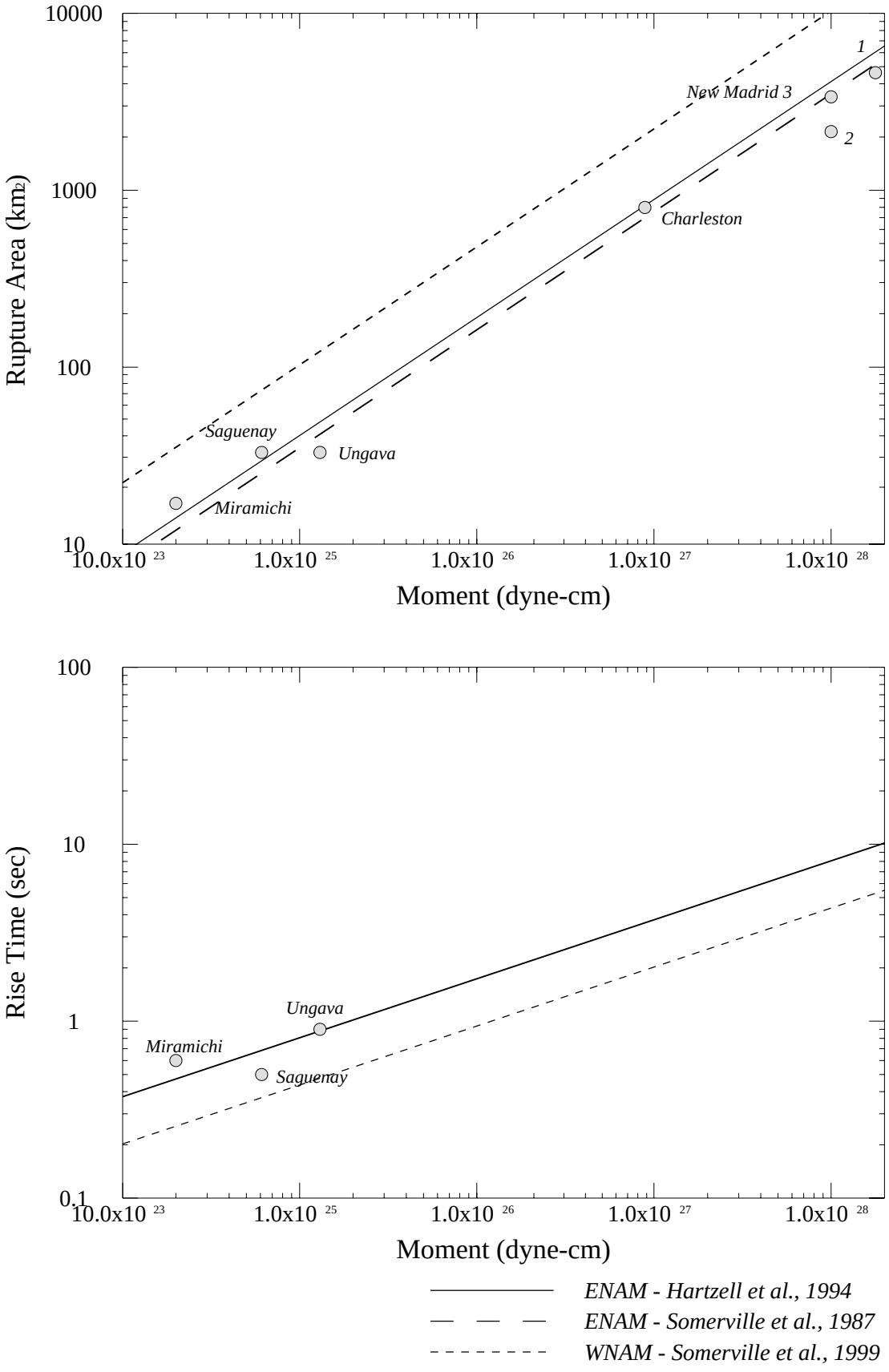

Figure 1. Scaling relations of eastern North American earthquakes and comparison with western North America.

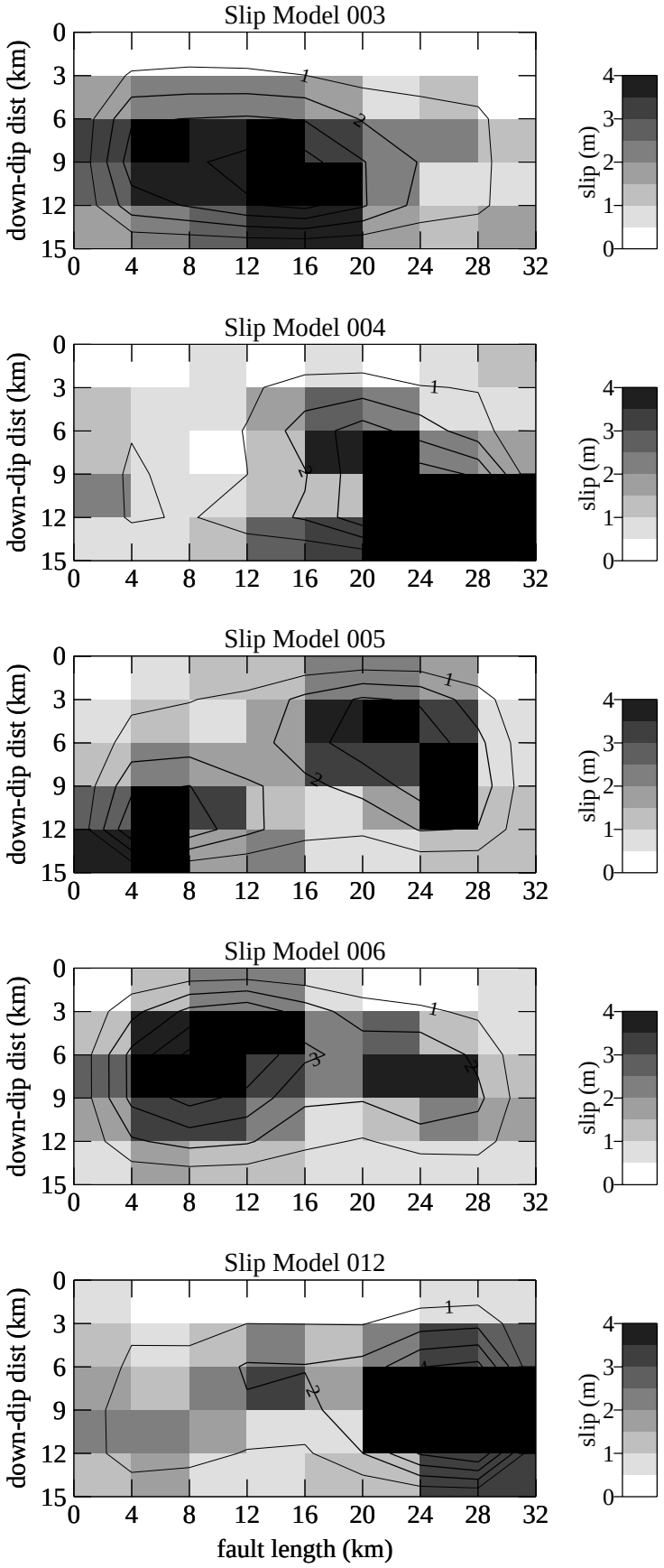

Figure 2. Slip models of magnitude 7 reverse faulting earthquakes in eastern North America.

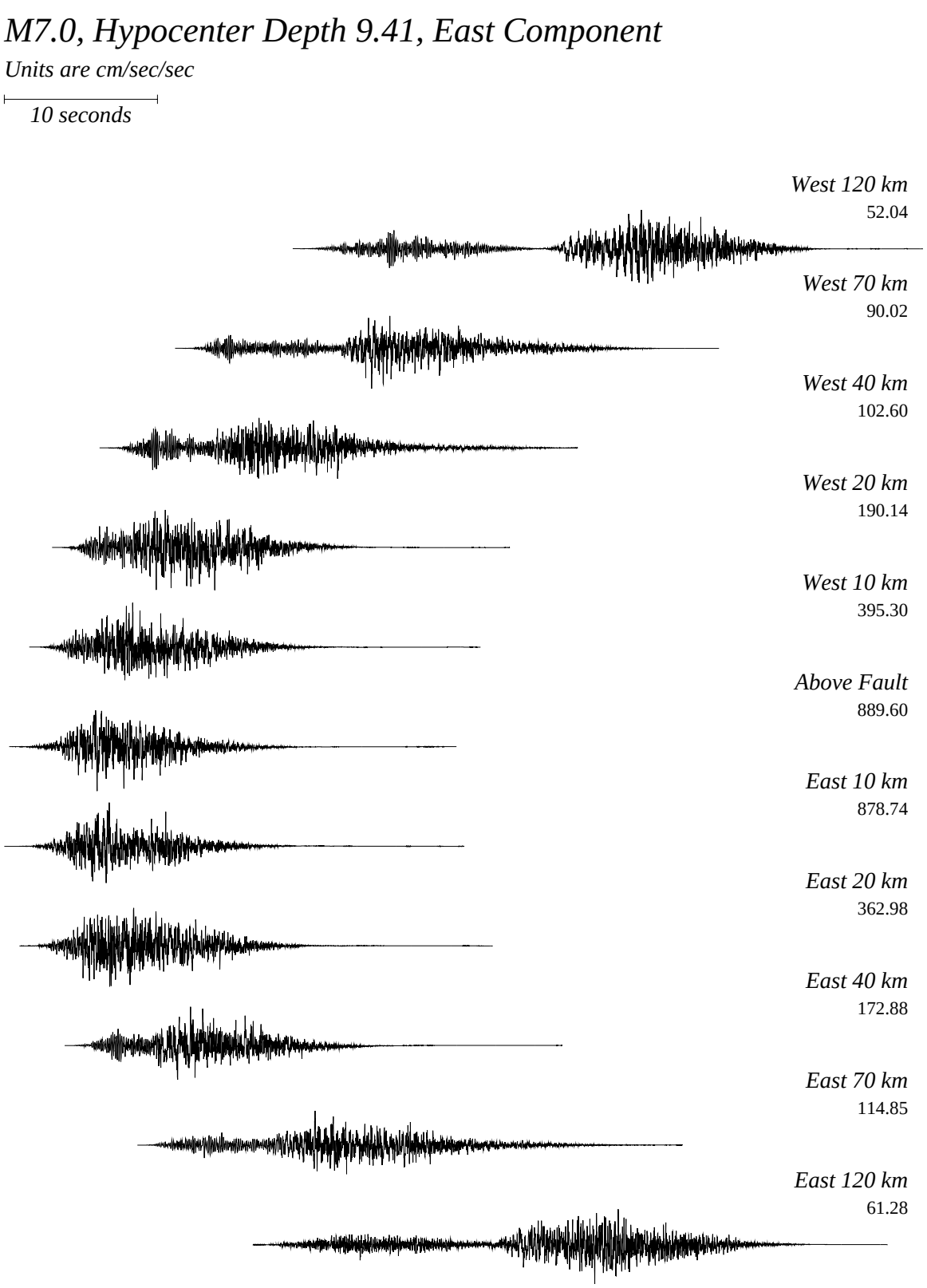

Figure 3. Profile of simulated accelerograms for a north-striking magnitude 7 reverse faulting earthquake in eastern North America. The distance from the fault on the foot wall (west) and hanging wall side (east) and peak acceleration are listed beside each accelerogram.

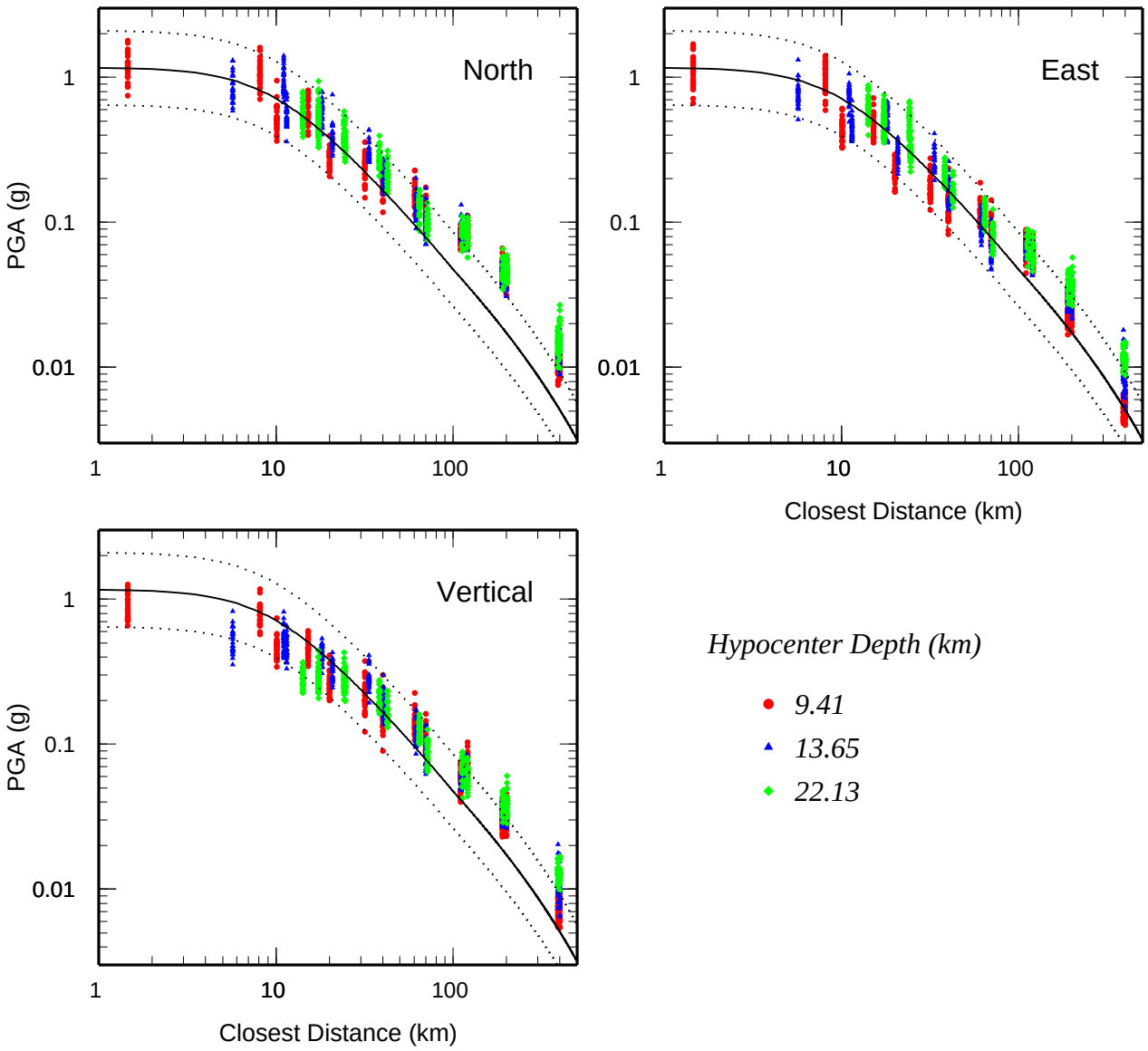

Slip Models 1-10, Azimuth=90 and 270

Attenuation Relation = Toro et al. 1997, Mid Continent Moment Magnitude Model

Figure 4. Attenuation of peak acceleration with distance from a magnitude 7 reverse faulting earthquake in eastern North American, compared with the model of Toro et al. (1997).

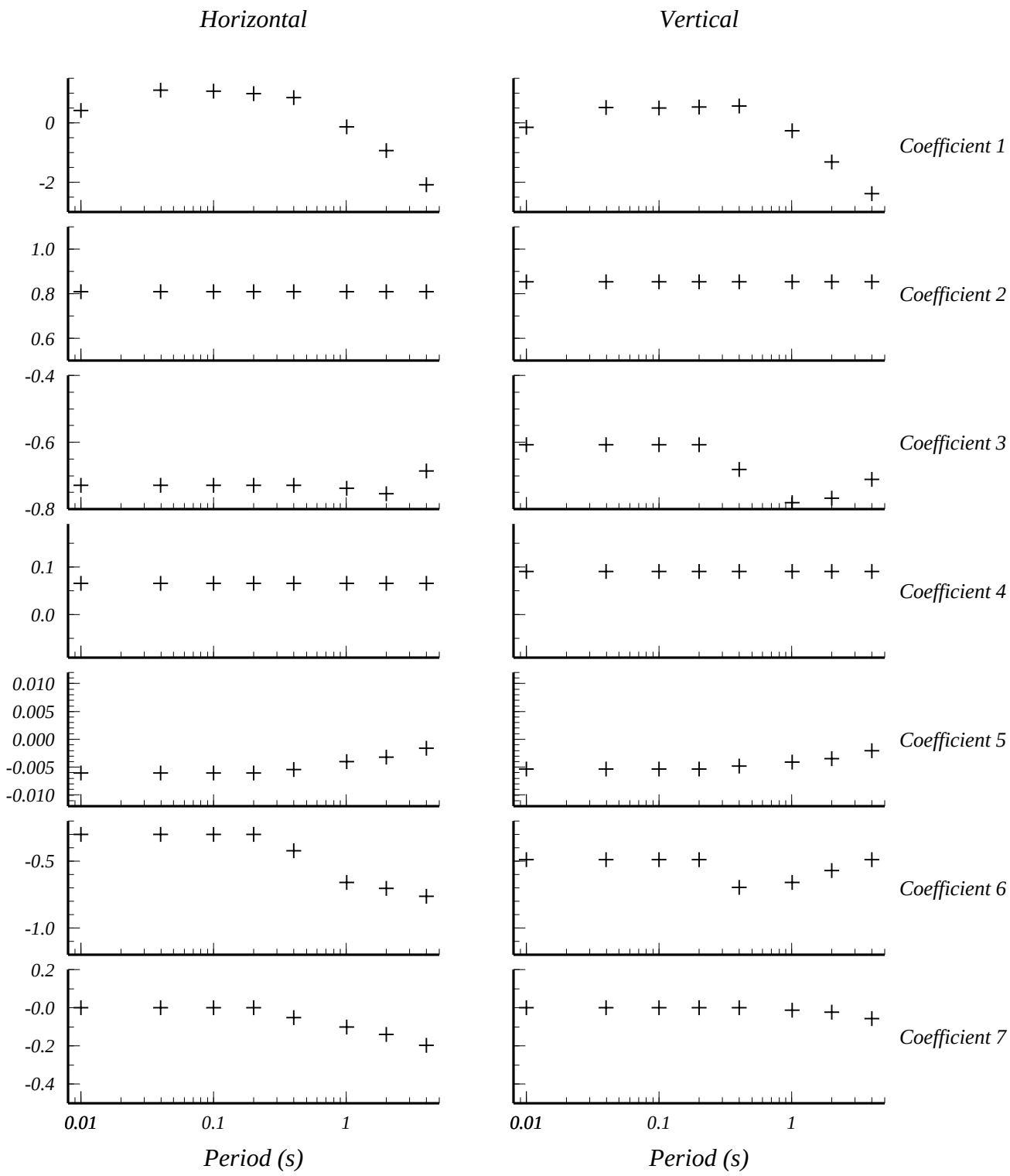

Figure 5. Coefficients of the nonrift ground motion attenuation model.

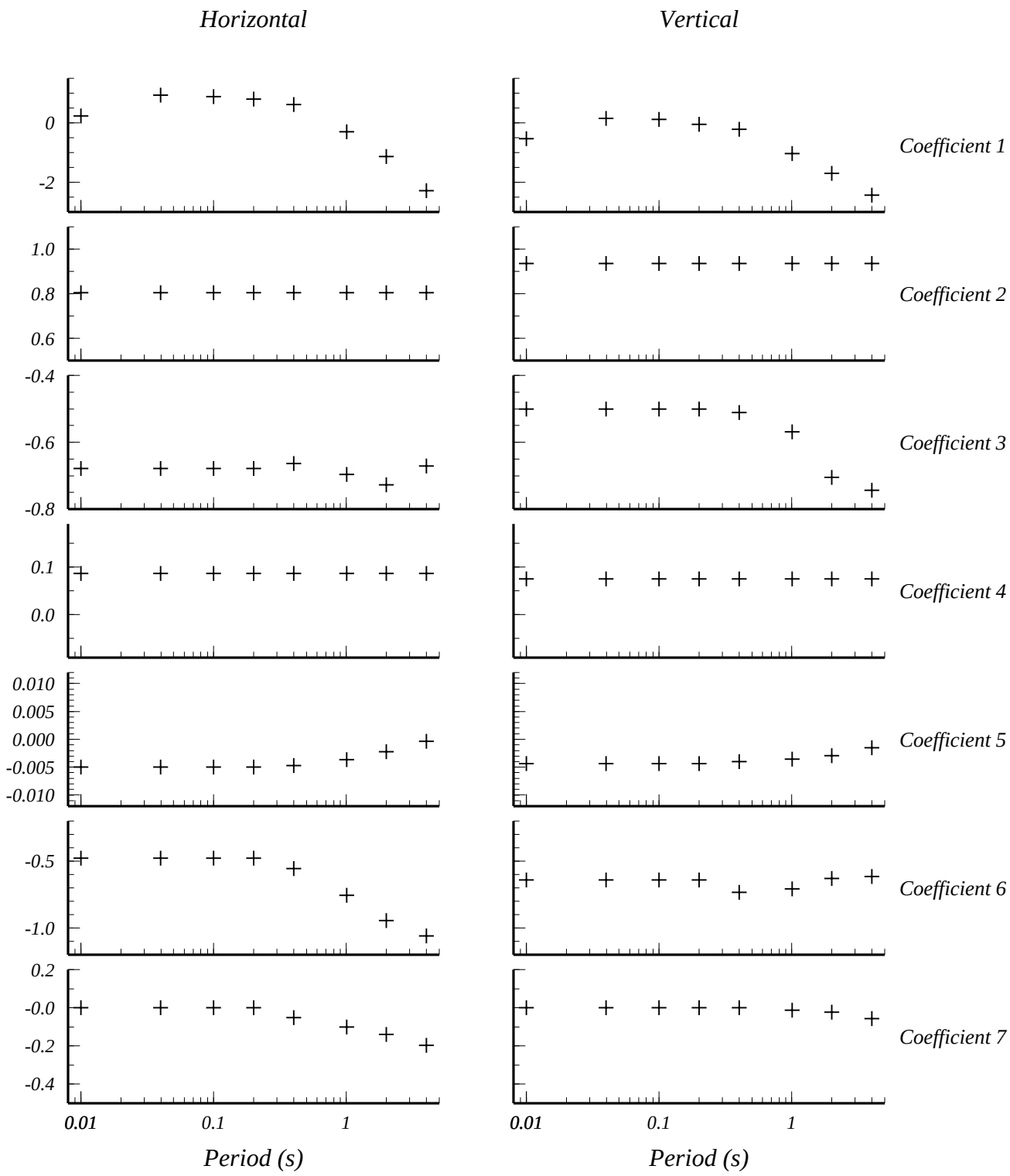

Figure 6. Coefficients of the rift ground motion attenuation model.

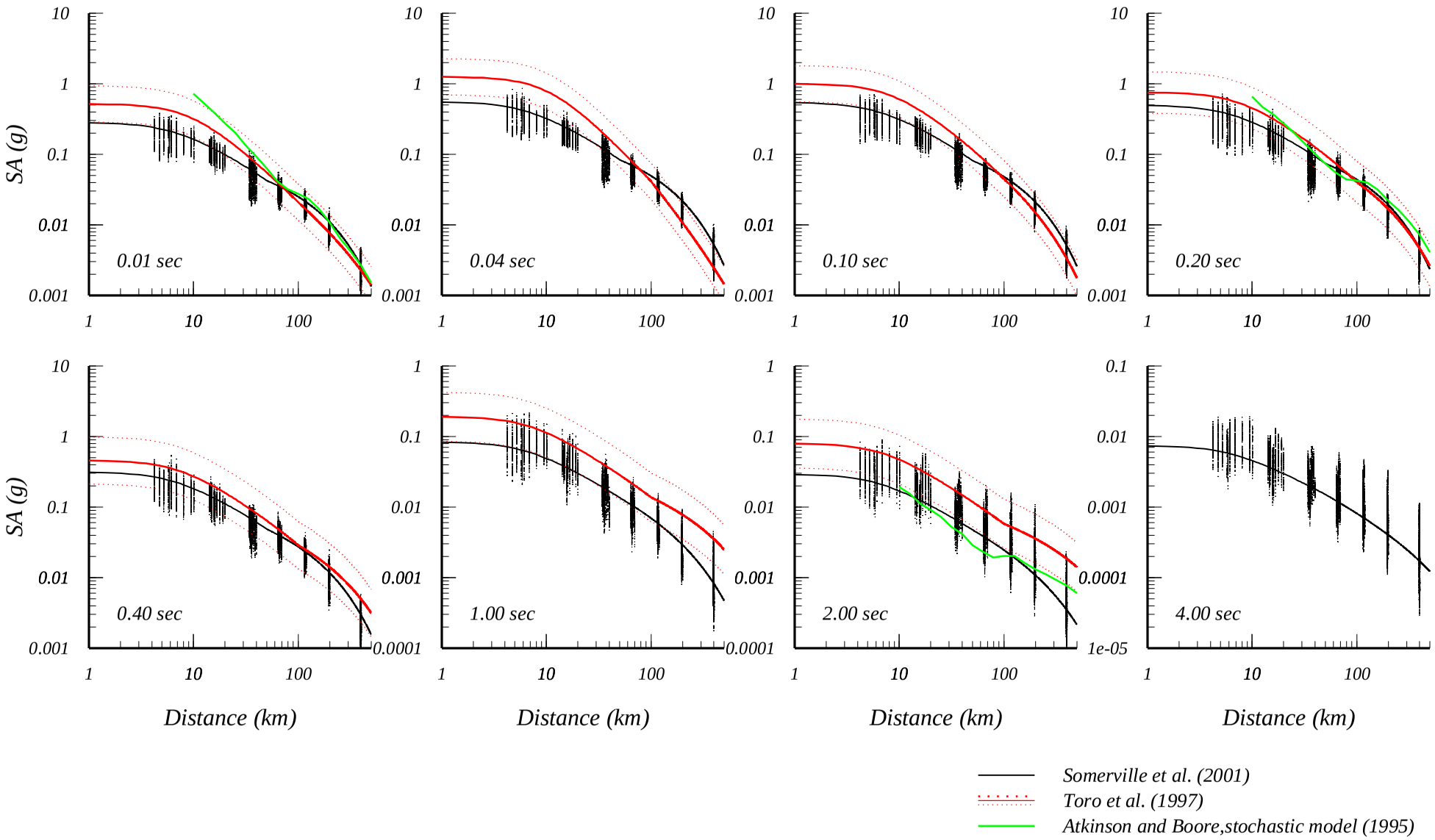

Figure 7. Horizontal ground motions model for non-rifted domains in ENA for a suite of periods for Mw 6.0. The simulation values on which the model is based are shown by dots. For some periods the model is compared with Toro et al. (1997) and Atkinson and Boore (1995) models.

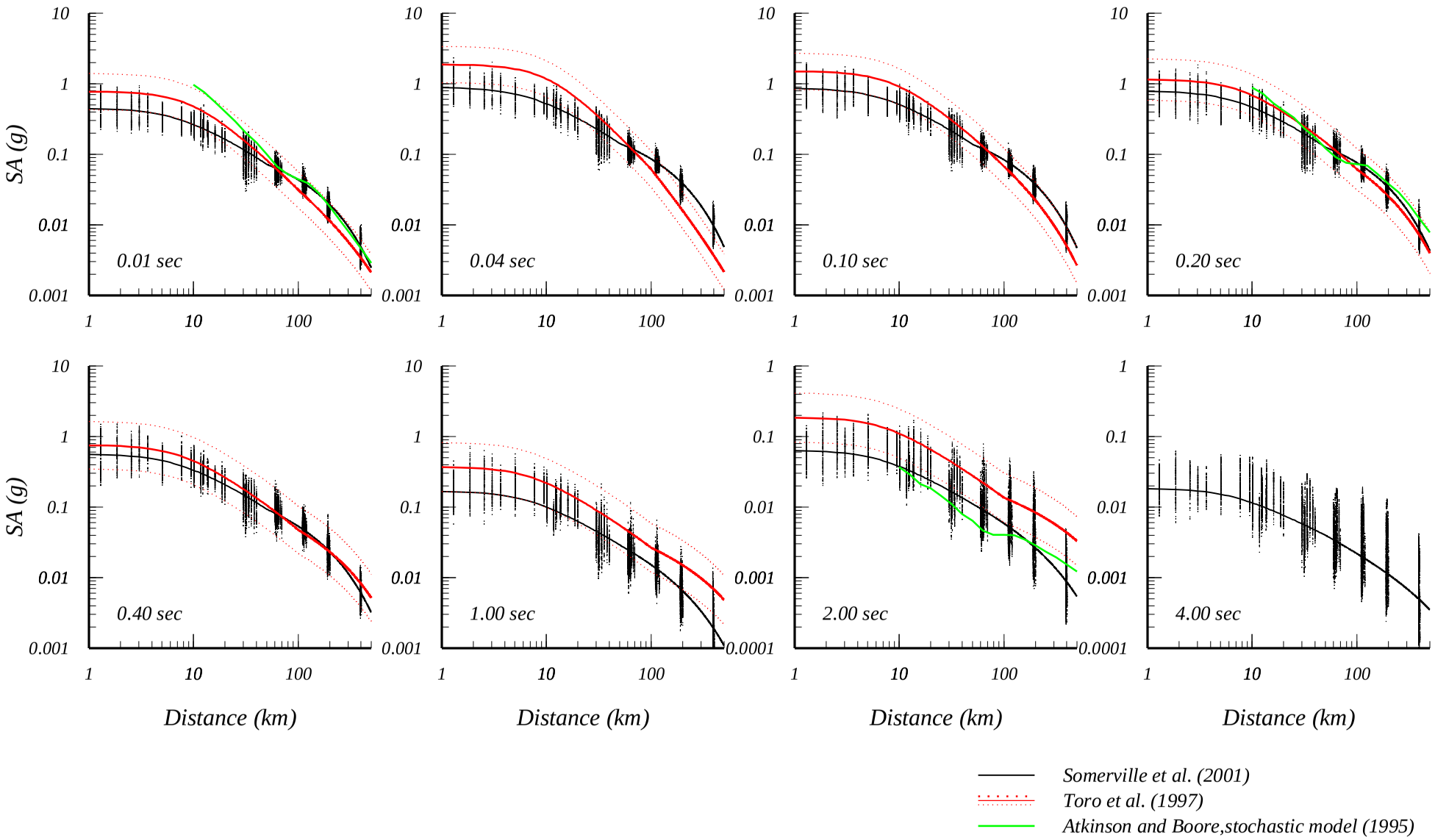

Figure 8. Horizontal ground motions model for non-rifted domains in ENA for a suite of periods for Mw 6.5. The simulation values on which the model is based are shown by dots. For some periods the model is compared with Toro et al. (1997) and Atkinson and Boore (1995) models.

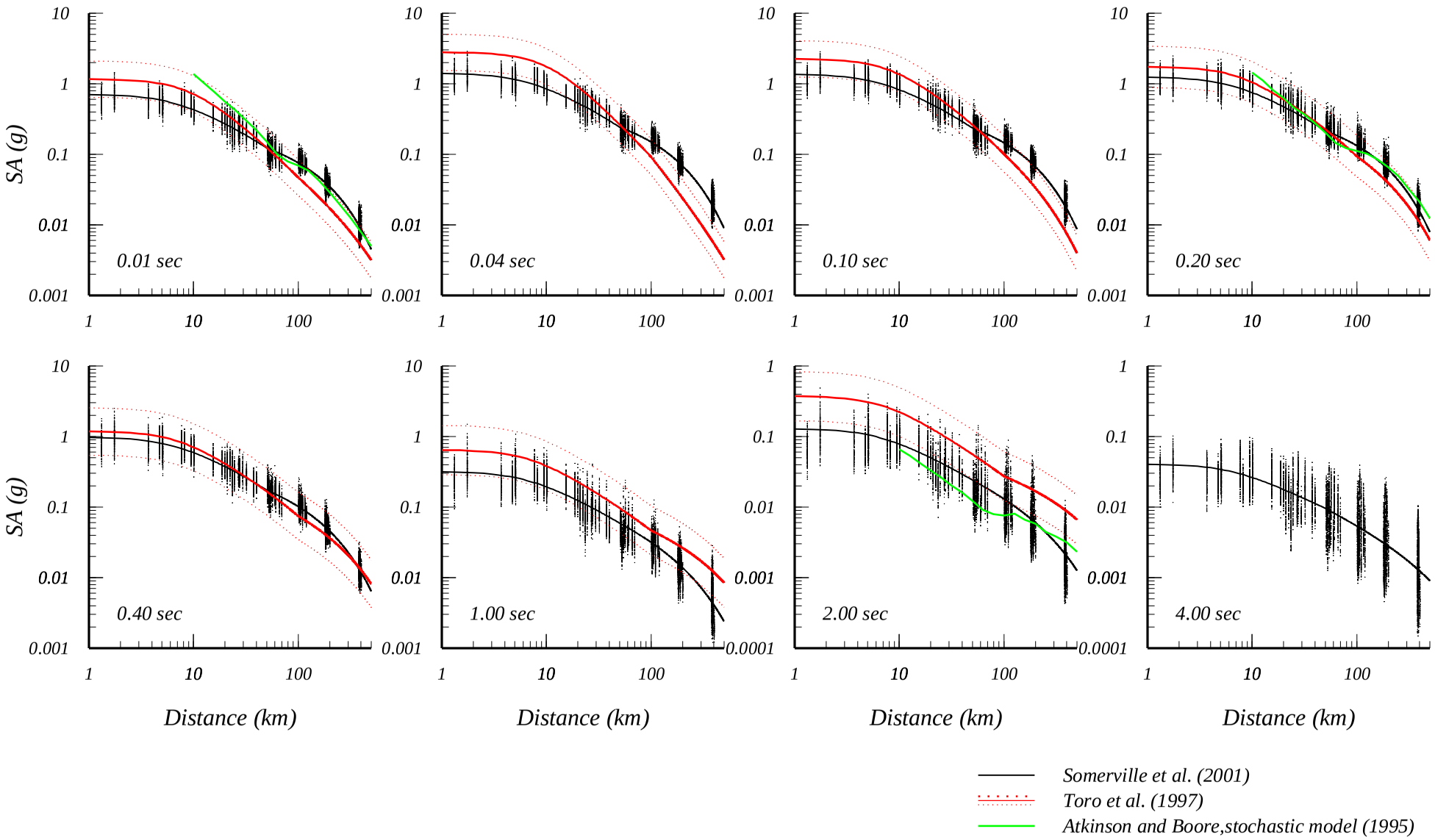

Figure 9. Horizontal ground motions model for non-rifted domains in ENA for a suite of periods for Mw 7.0. The simulation values on which the model is based are shown by dots. For some periods the model is compared with Toro et al. (1997) and Atkinson and Boore (1995) models.

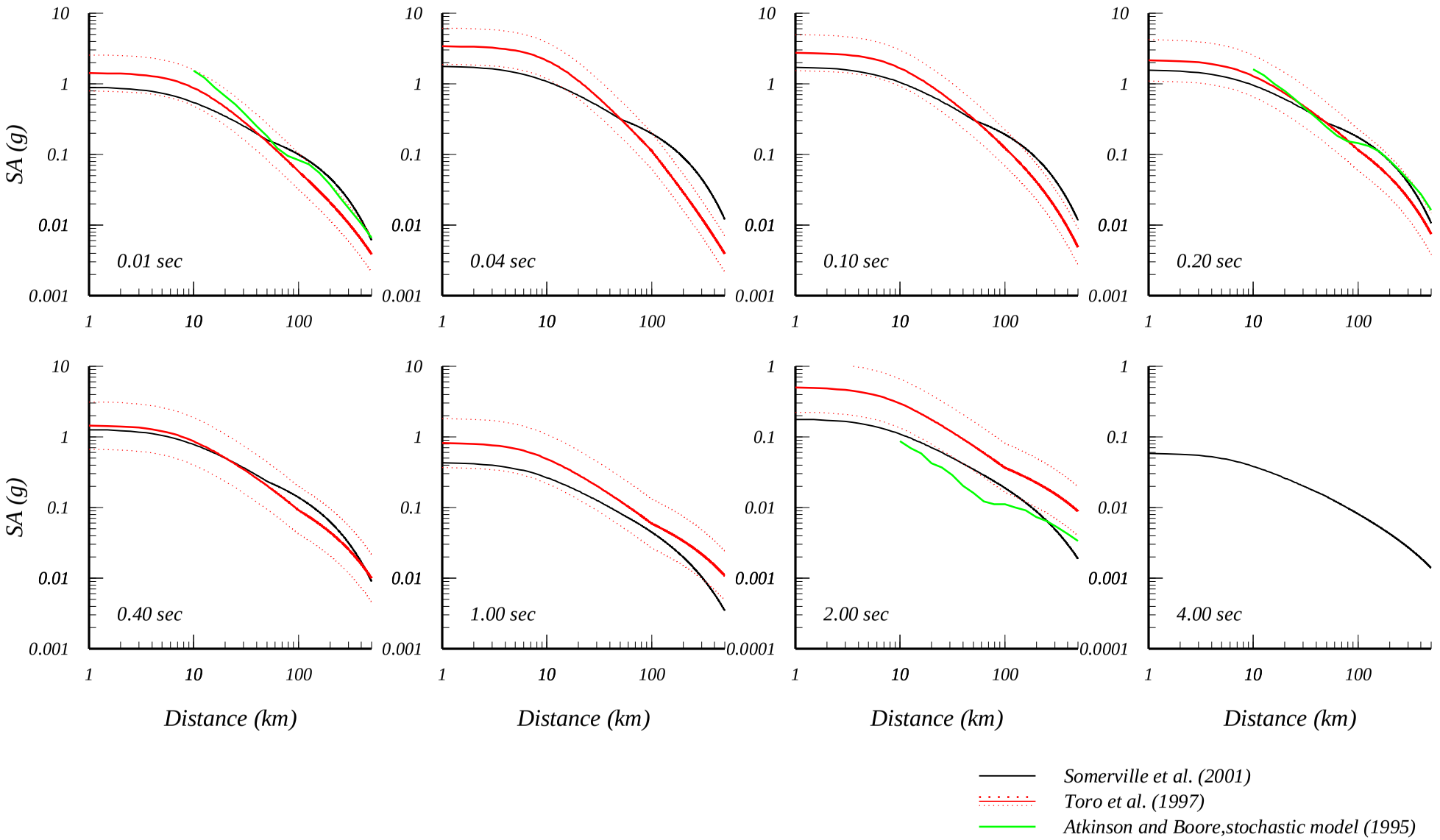

Figure 10. Horizontal ground motions model for non-rifted domains in ENA for a suite of periods for Mw 7.25. The simulation values on which the model is based are shown by dots. For some periods the model is compared with Toro et al. (1997) and Atkinson and Boore (1995) models.

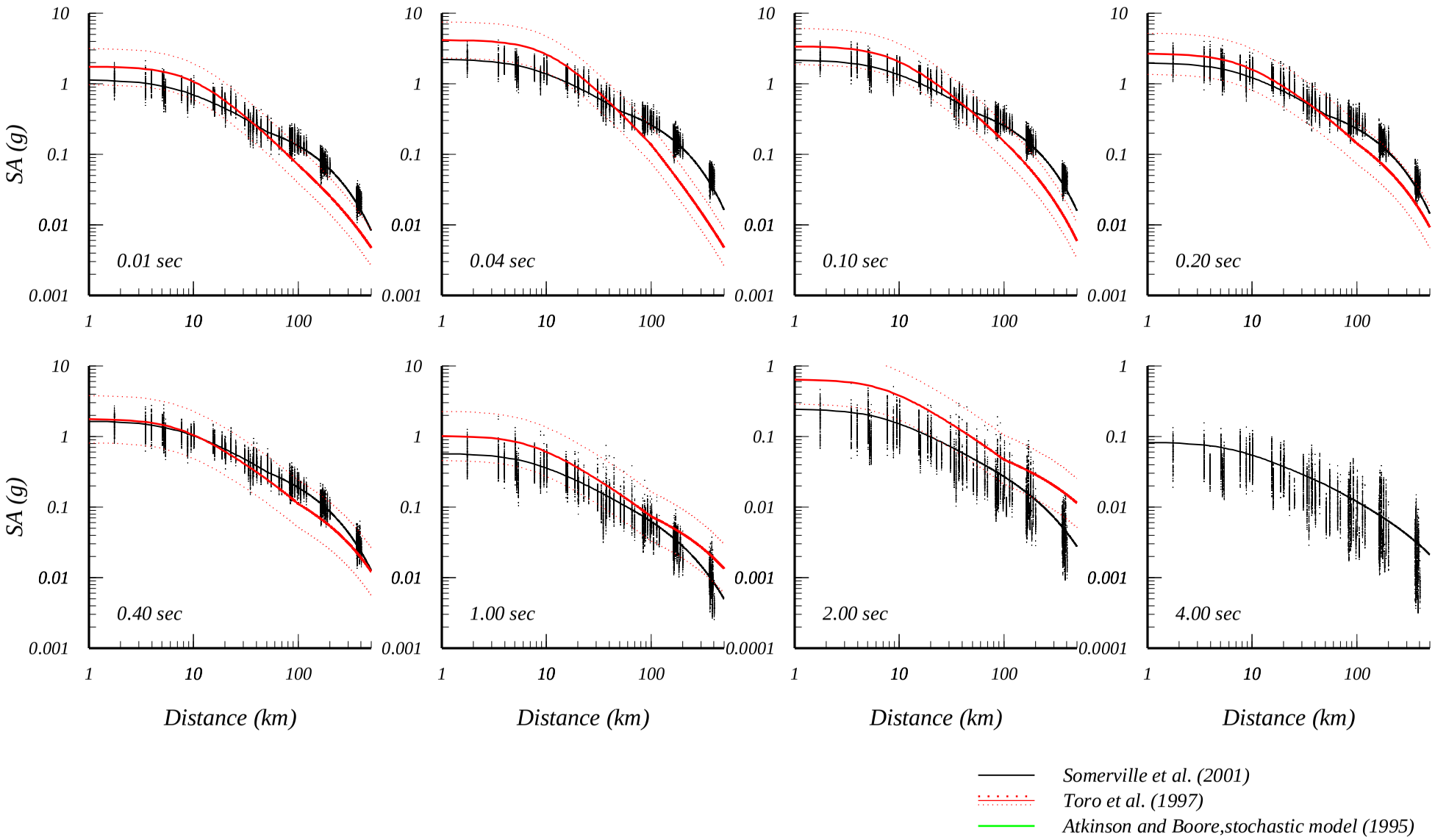

Figure 11. Horizontal ground motions model for non-rifted domains in ENA for a suite of periods for Mw 7.5. The simulation values on which the model is based are shown by dots. For some periods the model is compared with Toro et al. (1997) and Atkinson and Boore (1995) models.

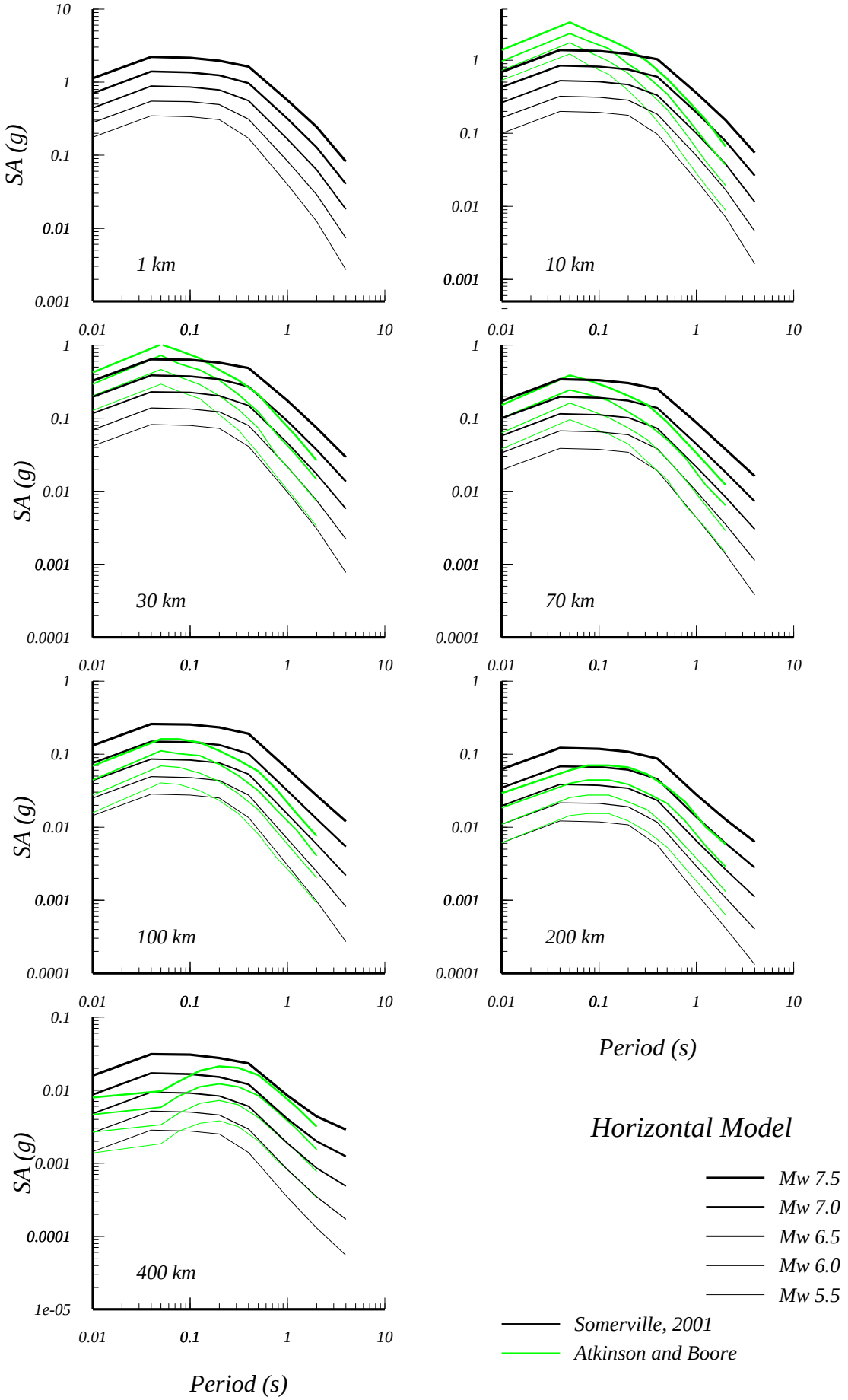

Figure 12. Non-rift model horizontal response spectral comparison with Atkinson and Boore.

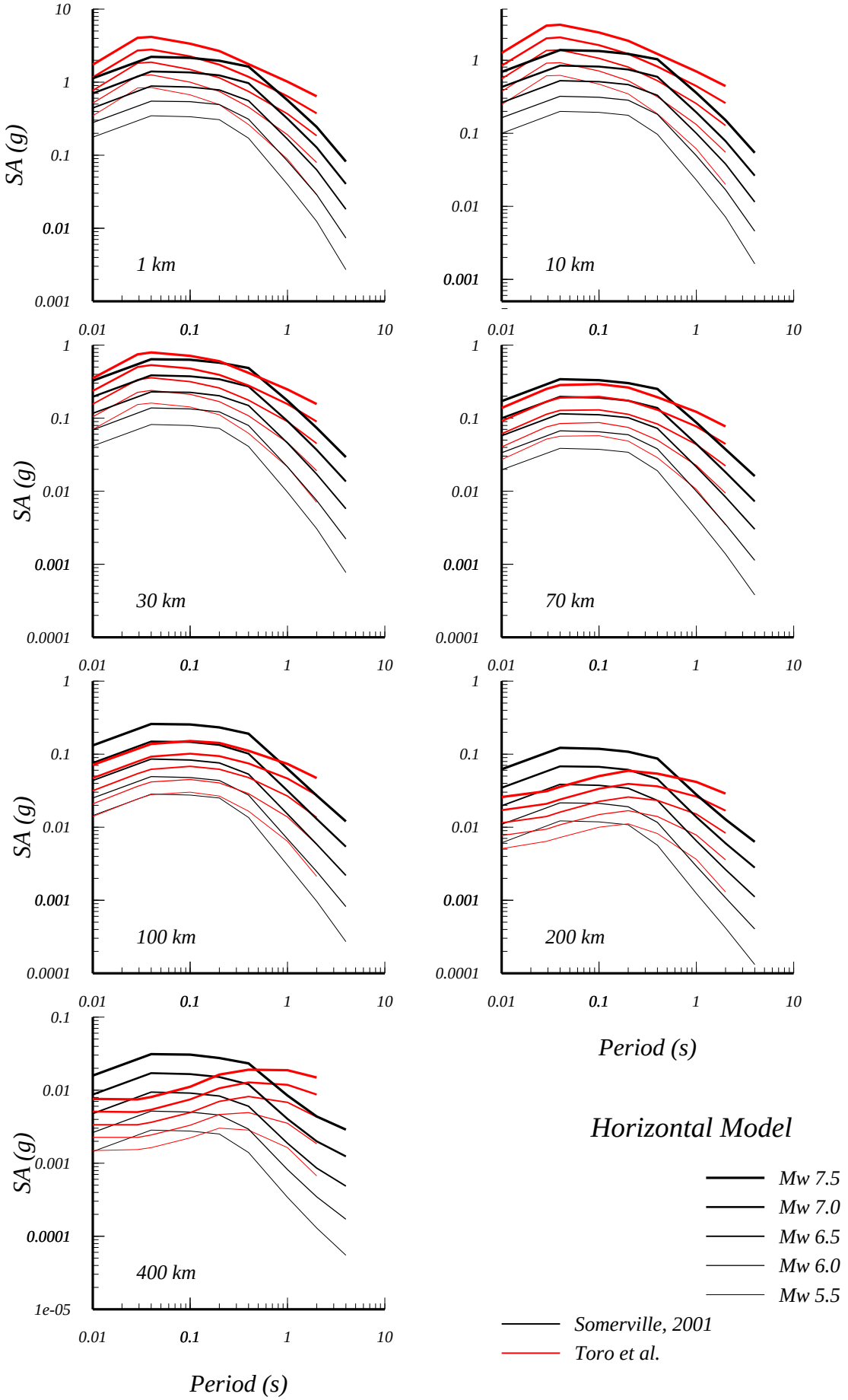

Figure 13. Non-rift model horizontal response spectral comparison with Toro et al..

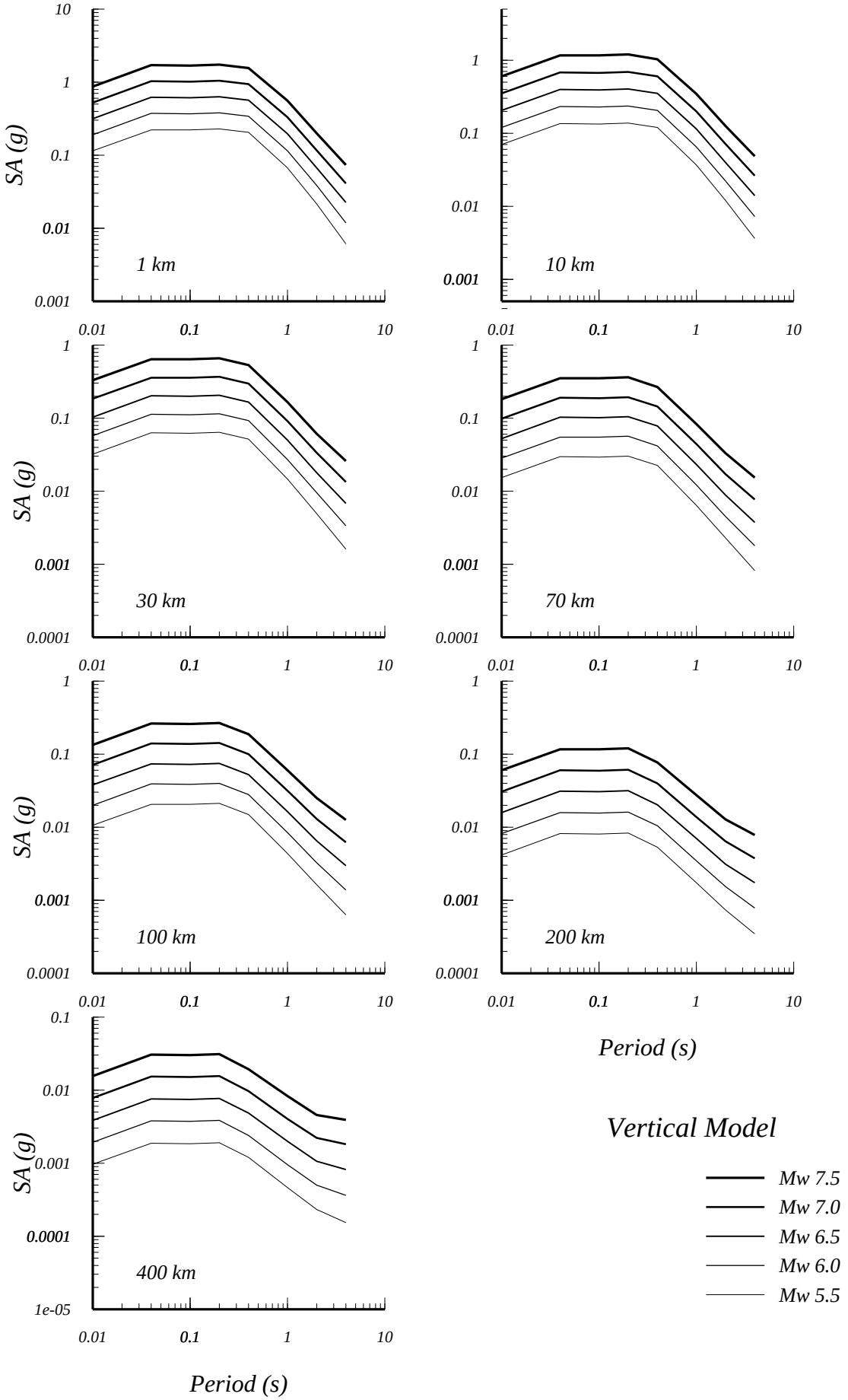

Figure 14. Non-rift model vertical response spectra.

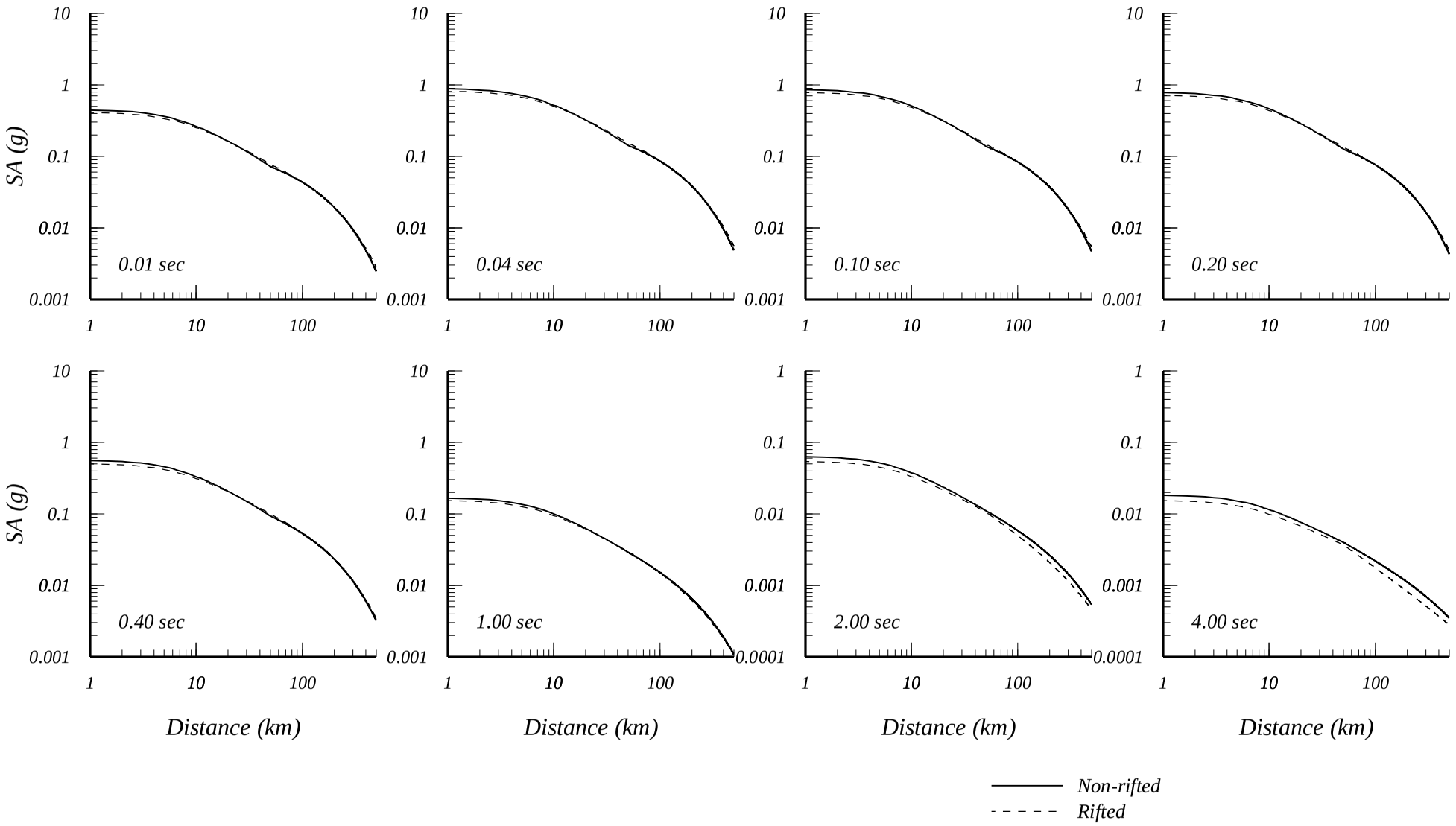

Figure 15. Horizontal ground motion models for non-rifted and rifted domains in ENA for a suite of periods for Mw 6.5.

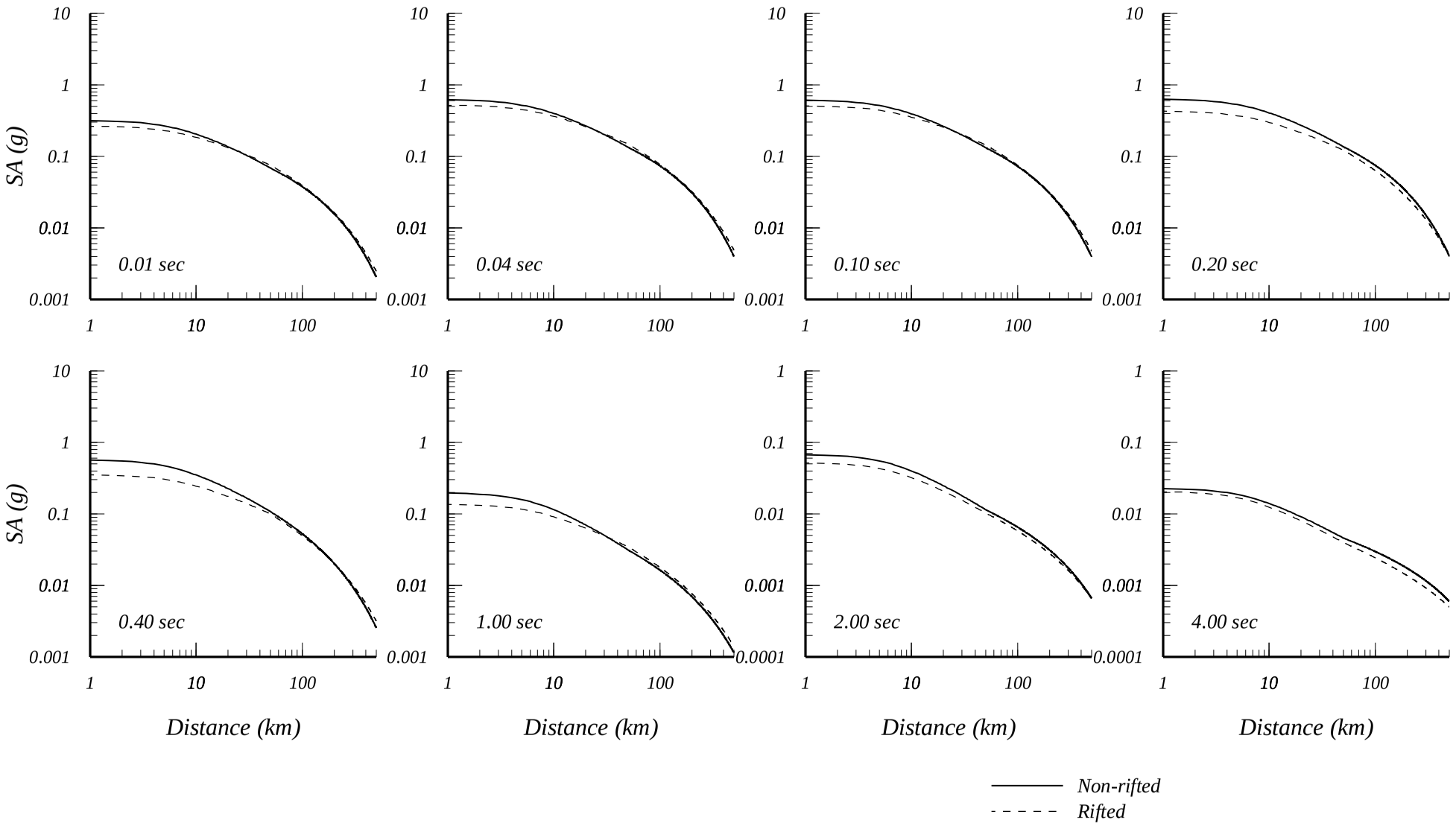

Figure 16. Vertical ground motion models for non-rifted and rifted domains in ENA for a suite of periods for Mw 6.5.

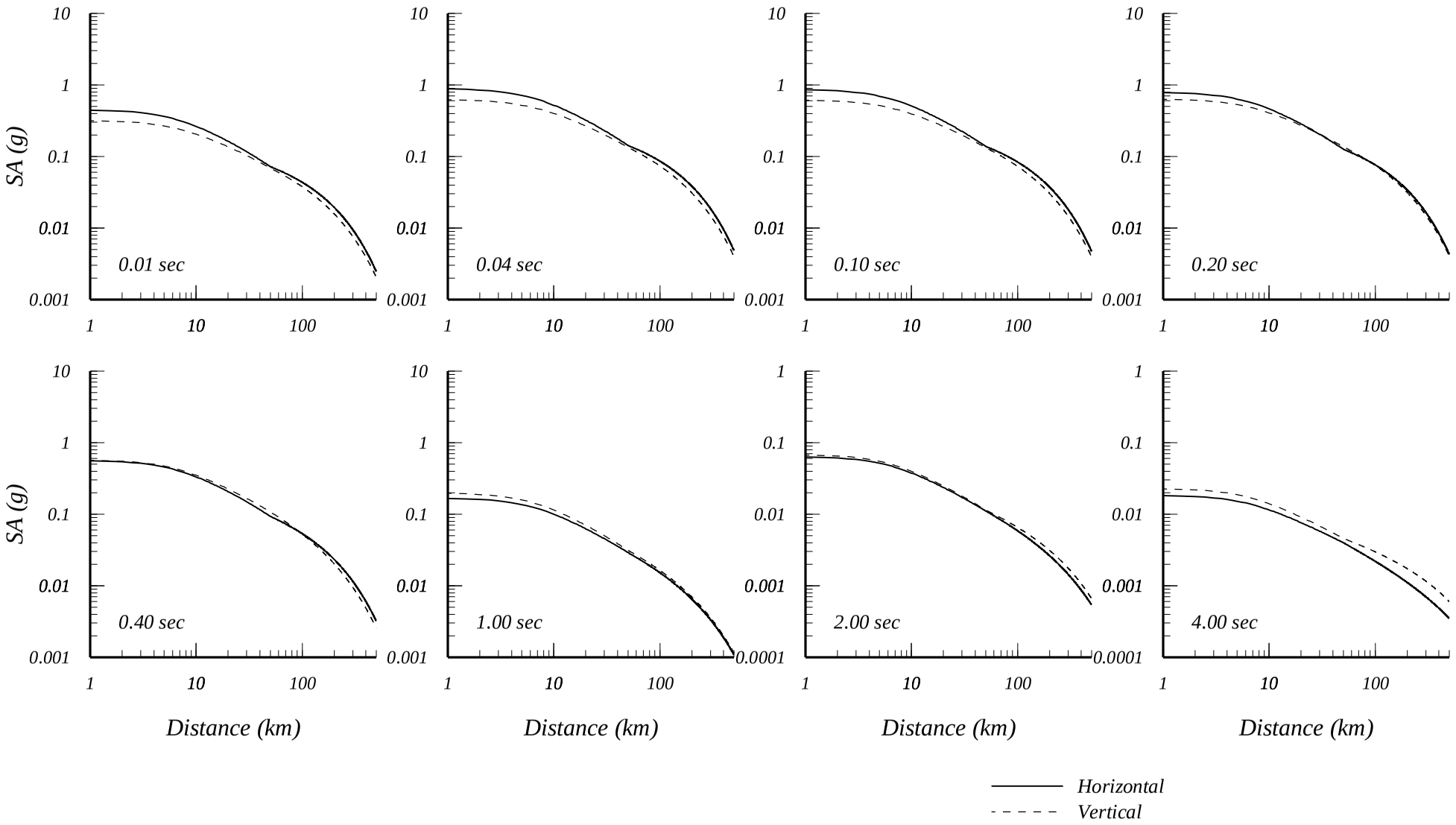

Figure 17. Horizontal and vertical ground motion model for non-rifted domains in ENA for a suite of periods for Mw 6.5.

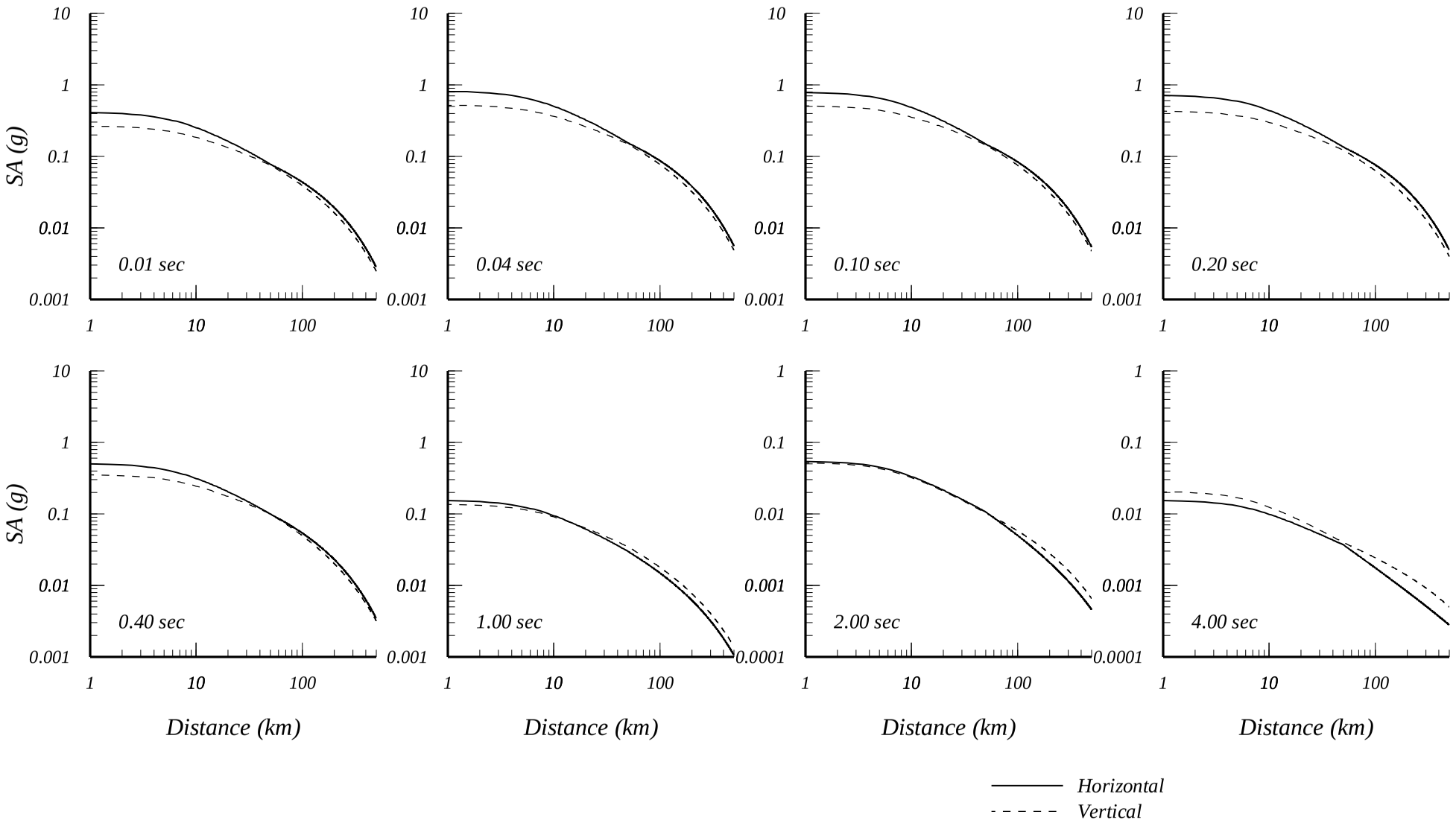

Figure 18. Horizontal and vertical ground motion model for rifted domains in ENA for a suite of periods for Mw 6.5.

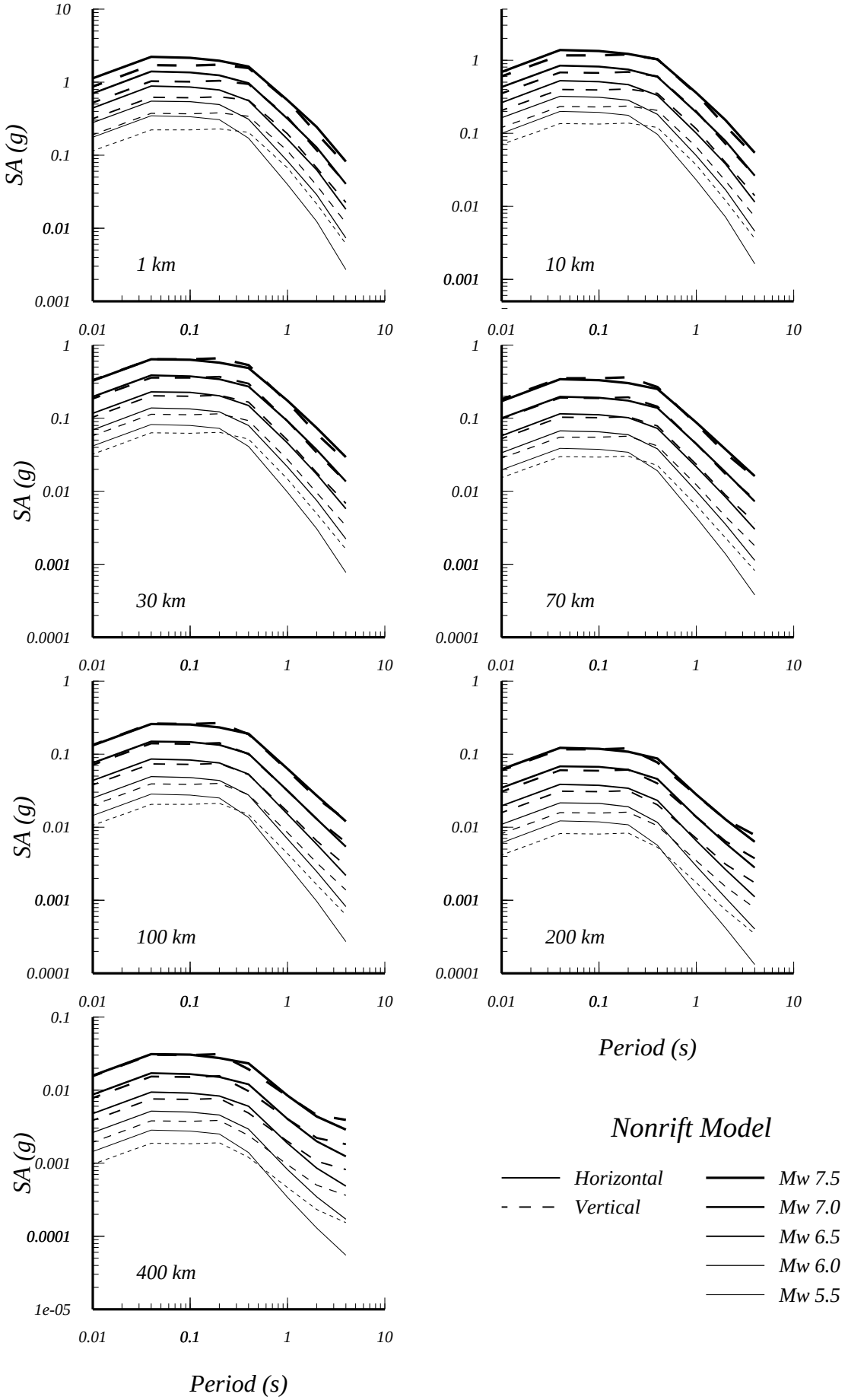

Figure 19. Nonrift response spectral model for a set of magnitudes and a suite of distances.

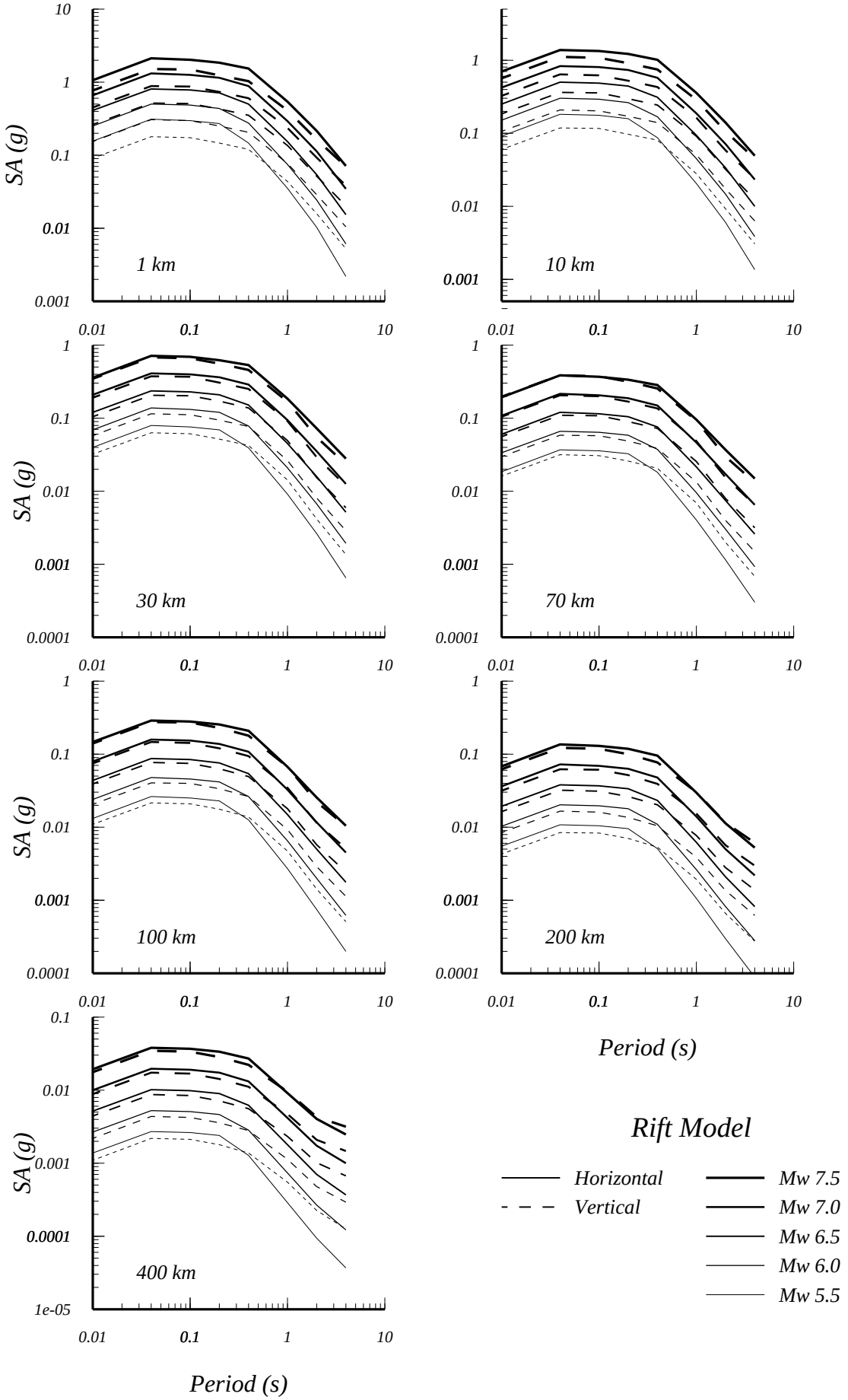

Figure 20. Rift response spectral model for a set of magnitudes and a suite of distances.

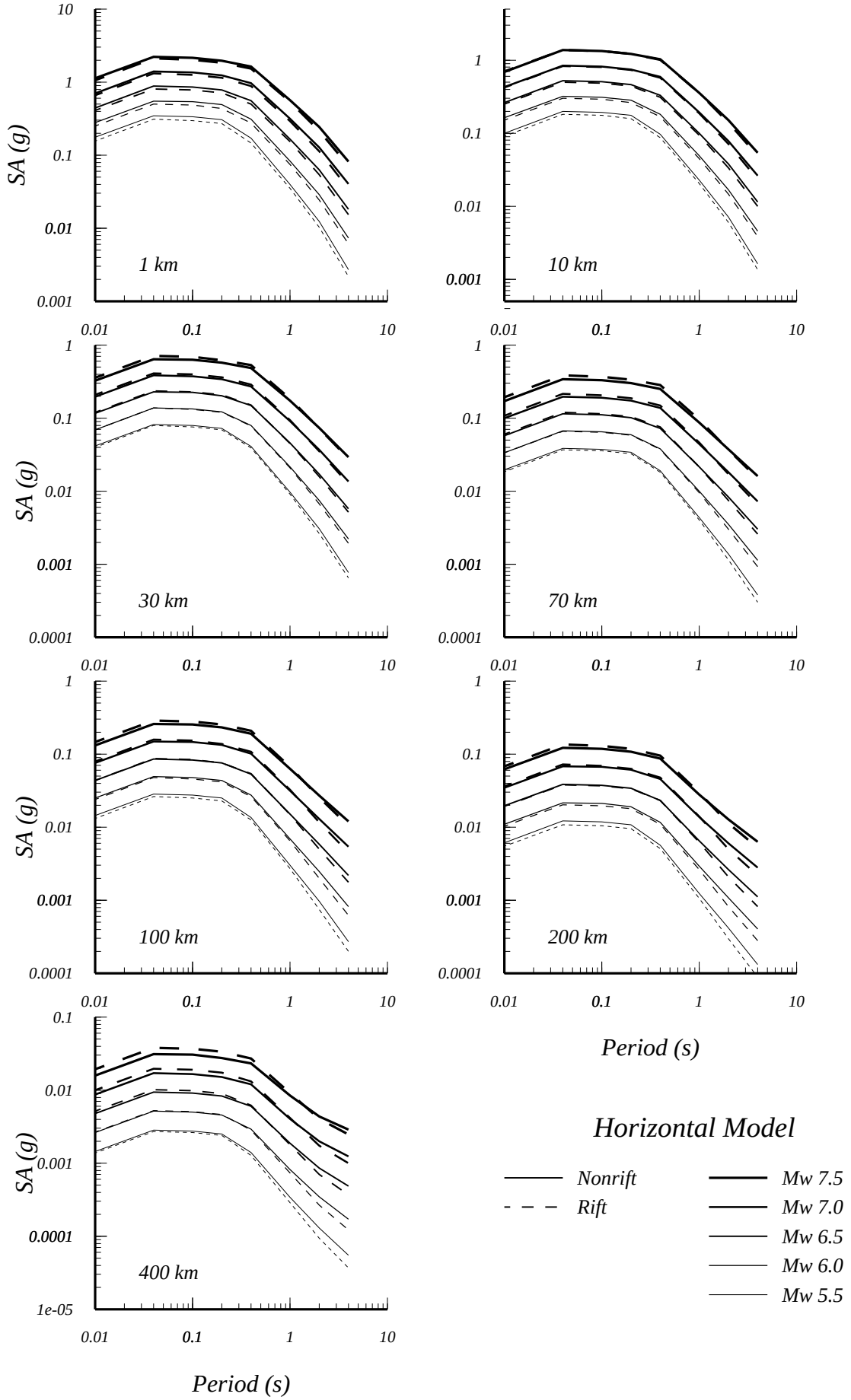

Figure 21. Horizontal response spectral model for a set of magnitudes and a suite of distances.

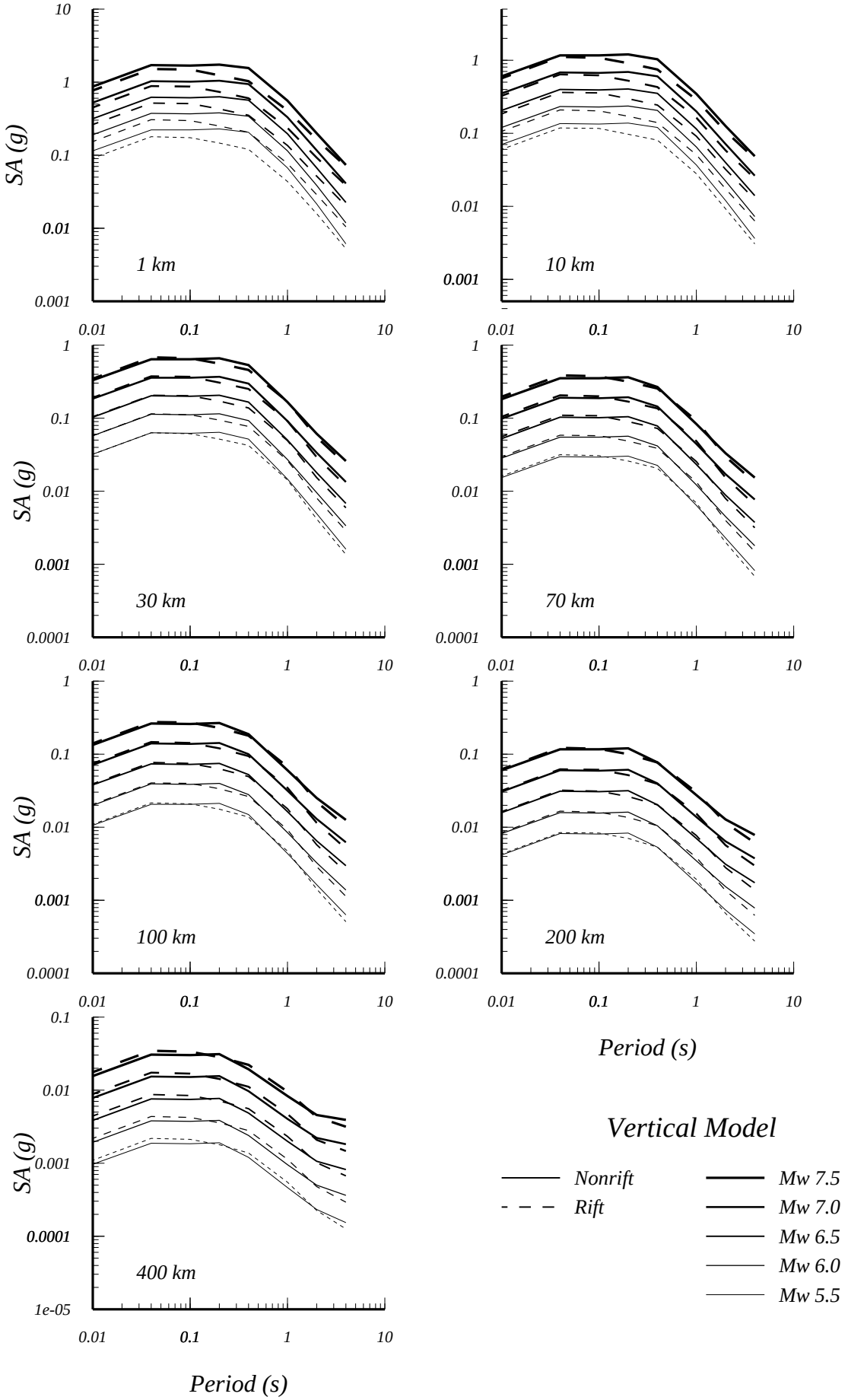

Figure 22. Vertical response spectral model for a set of magnitudes and a suite of distances.